

Investigation of particle and vapor wall-loss effects on controlled wood-smoke smog-chamber experiments

Qijing Bian¹, Andrew A. May², Sonia M. Kreidenweis¹, and Jeffrey R. Pierce^{1,3}

¹Department of Atmospheric Science, Colorado State University, Fort Collins, CO, USA

²Department of Civil, Environmental and Geodetic Engineering, the Ohio State University, Columbus, OH, USA

³Department of Physics and Atmospheric Science, Dalhousie University, Halifax, NS, Canada

Correspondence to: S. M. Kreidenweis (sonia@atmos.colostate.edu) and J. R. Pierce (jeffrey.pierce@colostate.edu)

Abstract

Smog chambers are extensively used to study processes that drive gas and particle evolution in the atmosphere. A limitation of these experiments is that particles and gas-phase species may be lost to chamber walls on shorter timescales than the timescales of the atmospheric processes being studied in the chamber experiments. These particle and vapor wall losses have been investigated in recent studies of secondary organic aerosol (SOA) formation, but they have not been systematically investigated in experiments of primary emissions from combustion. The semi-volatile nature of combustion emissions (e.g. from wood smoke) may complicate the behavior of particle and vapor wall deposition in the chamber over the course of the experiments due to the competition between gas/particle and gas/wall partitioning. Losses of vapors to the walls may impact particle evaporation in these experiments, and potential precursors for SOA formation from combustion may be lost to the walls, causing underestimates of aerosol yields. Here, we conduct simulations to determine how particle and gas-phase wall losses contributed to the observed evolution of the aerosol during experiments in the third Fire Lab At Missoula Experiment (FLAME III). We use the TwO-Moment Aerosol Sectional (TOMAS) microphysics algorithm coupled with the organic volatility basis set (VBS) and wall-loss formulations to examine the predicted extent of particle and vapor wall losses. We limit the scope of our study to the dark periods in the chamber before photo-oxidation to simplify the aerosol system for this initial study.

Our model simulations suggest that over one third of the initial particle-phase organic mass (~~3641~~%) was lost during the experiments, and ~~roughly over~~ half of this particle organic mass loss was from direct particle wall loss (~~5665~~% of the loss) with the remainder from evaporation of the particles driven by vapor losses to the walls (~~4435~~% of the loss). We perform a series of sensitivity tests to understand uncertainties in our simulations. Uncertainty in the initial wood-smoke volatility distribution contributes ~~2318~~% uncertainty to the final particle organic mass remaining in the chamber (relative to base-assumptions simulation). We show that the total mass loss may depend on the effective

saturation concentration of vapor with respect to the walls as these values currently vary widely in the literature. The details of smoke dilution during the filling of smog chambers may influence the mass loss to the walls, and a dilution of ~25:1 during the experiments increased particle organic mass loss by ~~6433~~6433% compared to a simulation where we assume the particles and vapors are initially in equilibrium in the chamber. Finally, we discuss how our findings may influence interpretations of emission factors and SOA production in wood-smoke smog-chamber experiments.

1 Introduction

Wood burning, including agricultural combustion and wildfires in forests, grasses and woodlands, is the major primary source of atmospheric carbonaceous particles globally, comprising black carbon (BC) as well as organic carbon material in both the particle and vapor phases. Wood smoke is known to have important health (Naeher et al., 2007; Jassen, 2012; Johnston et al., 2012) and climate effects (Bond et al., 2013), yet the aerosol emission estimates for wood burning (mainly open burning) of $33800 \text{ Gg}^{-1} \text{ yr}^{-1}$ have an uncertainty ranging from a factor of 0.6 to 4 (Bond et al., 2013). The net effect of the climate forcing from biomass burning aerosol has been estimated in some studies to be nearly zero or negative due to the dominant cooling direct effect of primary organic aerosol (POA) over the warming from BC, as well as an indirect cooling effect from the particles' interactions with clouds by modifying the cloud albedo (Bond et al., 2013). ~~The net effect of the climate forcing from biomass burning aerosol has been estimated in some studies to be nearly zero or negative due to the dominant cooling direct effect of primary organic aerosol (POA) over the warming from BC, as well as a cooling effect from the particles' interactions with clouds (Bond et al., 2013).~~ Others have argued that biomass burning may still cause a net global warming because warming effects (e.g. cloud absorption effects, semi-direct effects, and aerosol absorption) might exceed the cooling effects (Chung, et al., 2012; Jacobson, 2014). Thus, the climate effects of biomass burning aerosol are highly uncertain. In radiative forcing estimates, the size, composition and morphology of biomass burning particles are important parameters (Sakamoto et al., 2015; Giordano et al., 2015). In-plume coagulation, semi-volatile POA evaporation, and condensation of low-volatility secondary organic vapor onto the pre-existing aerosols in the atmosphere generally govern the particle size evolution during the smoke transport (Jimenez et al., 2009; DeCarlo et al., 2010; Sakamoto et al., 2015). In addition, nucleation of particles has also been observed in both chamber and field studies of biomass burning during the photo-oxidation process (Rissler et al., 2006; Hennigan, et al., 2012).

POA from wood smoke has been demonstrated to be semi-volatile in recent experiments, and thus some POA will evaporate during dilution of a smoke plume (May

et al., 2013b). Related experiments have shown that photo-oxidation of wood smoke in smog chambers may more than double the organic aerosol mass concentration, but in some experiments the total organic aerosol mass concentration had a net loss (Grieshop et al., 2009; Hennigan, et al., 2011; Ortega et al., 2013; Platt et al., 2013).
5 Estimates of secondary organic aerosol (SOA) formation from observations in ambient plumes also have mixed results, with some plumes showing little or no formation (Capes, et al., 2009; Cubison et al., 2011; Akagi et al., 2012; May et al., 2015; Sakamoto et al., 2015) and some showing significant formation (Yokelson et al., 2009; DeCarlo et al., 2010; Vakkari et al., 2014), although different studies sampled the
10 plumes during different stages of evolution, which may explain some of the discrepancies. Accurate simulation of wood-smoke particle mass evolution (i.e., POA and SOA) in chemical transport models is necessary to estimate the climate and health effects of wood-smoke emissions.

Photo-chemical oxidation of semi-volatile organic species (species that have non-trivial
15 partitioning in both the particle and vapor phases) and intermediate volatility organic species (species that are somewhat more volatile than semi-volatile species and primarily exist in the vapor phase) to lower volatility SOA is believed to be the major pathway of SOA formation during wood-smoke particle aging (Robinson et al., 2007; Grieshop et al., 2009; Huffman et al., 2009; Ortega et al., 2013; Jathar et al., 2014). As
20 wood-smoke plumes dilute during transport, POA may evaporate from particles and SOA production enhanced by oxidation of these organic vapors. The volatility distribution of the biomass burning vapor and particles may change correspondingly with increasing distance to the emission sources as POA evaporates and SOA forms.

Teflon smog chambers have been extensively used for emission and photochemistry
25 studies. It has been known for decades that particle wall loss in these chambers may dominate the changes in the particle distribution under certain experimental conditions (Crump and Seinfeld, 1981; McMurry and Grosjean, 1985; McMurry and Rader, 1985). Particle wall losses are quantified and used to correct observed aerosol concentrations to deduce the SOA formation in smog chamber studies (Weitkamp et al., 2007;
30 Hennigan et al., 2011). In these studies, semi-volatile vapors are generally assumed to be in equilibrium with particles deposited to the walls, but not in equilibrium with the walls themselves. While vapor wall loss has also been explored for decades (e.g. McMurry and Grosjean, 1985), its magnitude has been relatively unconstrained (compared to particle-phase wall losses), and it has not accounted for in most smog-
35 chamber studies. However, recent studies of vapor wall losses have shown that organic vapors have absorptive partitioning behavior to the Teflon walls of the smog chambers, and that this absorption may be modeled using Henry's law (Loza, et al. 2010; Matsunaga and Ziemann, 2010; Zhang et al., 2015). Zhang et al. (2014) showed that vapor wall losses may lead to underestimates of SOA formation from both biogenic and

anthropogenic SOA precursor gases in some experiments by a factor of 4 for their experimental conditions.

5 In controlled wood-smoke smog-chamber experiments, particle and vapor wall losses may complicate the estimates of particle-phase mass loss and SOA production. Vapor wall loss can force vapor concentrations to be lower than their equilibrium concentrations with respect to the particle phase. This deviation from equilibrium will cause evaporation of semi-volatile POA and lead to particle-phase mass loss beyond direct losses of the particles to the walls. Furthermore, losses of semi-volatile and intermediate volatility vapors to the walls will bias experimental SOA formation. Thus, 10 both particle-phase and vapor-phase wall losses must be considered in wood-smoke smog-chamber experiments, yet to our knowledge, no such estimates are currently available.

The goal of this study, therefore, is to simulate the vapor and particle wall losses of wood-smoke POA that is introduced into a smog chamber, based on current knowledge 15 of vapor and particle loss rates, to quantify their relative importance. For model initialization and validation, we use observations from the third Fire Lab At Missoula Experiments (FLAME III). We perform a series of sensitivity studies on unknown parameters to evaluate the model uncertainties and their effect on the predicted POA partitioning behavior. As our analysis of POA contains several dimensions of wall-loss 20 uncertainties, we limit the scope of this paper to POA and primary vapors, and we will investigate SOA production uncertainties in a future paper. In section 2, we describe the experimental procedure and model simulation. In section 3, we present the results of the base simulation and sensitivity tests and discuss the potential influence of wall and vapor losses on SOA formation. Section 4 summarizes the results and gives 25 recommendations for future work.

2 Methods

2.1 Experimental description

Smog-chamber experiments to investigate wood-smoke POA partitioning and wood-smoke SOA formation were carried out during the FLAME III study at the USDA/USFS 30 Fire Sciences Laboratory (FSL) in Missoula, Montana during September-October 2009 (Hennigan et al., 2011; May et al., 2013b; May et al. 2014). Eighteen types of fuels were studied that represent North American vegetation that is typically burned in wild or prescribed fires. Fuel samples (0.3-1.0 kg) were arranged on a fuel bed in the FSL combustion chamber (12.4 m × 12.4 m × 19.6 m, 3014 m³, Table 1), ignited electrically, 35 and combusted in open burning. After burn completion and subsequent mixing of emissions in the FSL combustion chamber for ~30 min, a smoke sample was withdrawn and introduced to the CMU smog chamber, a Teflon bag with a volume of ~7 m³,

through a heated transfer line with an average 94% particle-transmission efficiency between 50-400 nm (Hennigan et al., 2011). Filling commenced until aerosol concentrations of $\sim 50 \mu\text{g m}^{-3}$ were achieved, representing $\sim 25\times$ dilution from the conditions present in the FSL combustion chamber (dilution was a 2-step process, including roughly 7:1 dilution in Dekati ejector dilutors and bag filling for the remainder, Hennigan et al., 2011). Sampling from the CMU smog chamber occurred through a thermodenuder (May et al., 2013a) that was upstream of an Aerodyne quadruple aerosol mass spectrometer (Q-AMS) and a scanning-mobility particle sizer (SMPS). Nonrefractory speciated submicron aerosol mass (OA, SO_4^{2-} , NO_3^- , NH_4^+ , and Cl^-) was characterized by the Q-AMS, black carbon (BC) was determined by a 7-channel Aethalometer at 880 nm, and the number size distribution between diameters of 10.9 and 478.3 nm was measured by the SMPS. In this paper, we define the total submicron aerosol mass (TA) as the sum of OA, SO_4^{2-} , NO_3^- , NH_4^+ , Cl^- , and BC, and we define the organic fraction (OF) as the ratio of OA / TA. To reconcile the volume and mass measurements between SMPS and AMS, we compute an effective density (DeCarlo et al., 2004) of the particles for each burn by dividing the total AMS mass by the total SMPS volume. For this purpose, the SMPS size distribution was extrapolated to 1 μm , the upper size limit for the AMS, using a single lognormal fit of the SMPS volume distribution (Figure S1). While the volume distribution appears lognormal up to 400 nm (upper limit of the SMPS), we do not know for sure if the distribution follows the fit lognormal curve at larger sizes. Therefore, these calculated effective densities represent the combined effect of non-unity collection efficiencies in the AMS, particle density, and particle shape, but contain uncertainties due to the size extrapolation. We use the effective densities to translate modeled mass distributions to the measured values. Measurements of primary gas and particle concentrations were conducted for ~ 75 min after smoke was well mixed in the smog chamber before UV lights were turned on for photo-oxidation. It is this period before photo-oxidation and after bag filling, during which the initial aerosol was characterized, that we study in this paper. Further, we use the term "POA" to describe the mass concentration of organic compounds observed in the particle phase at the start of this period, as measured by the Q-AMS (i.e., OA at time=0).

2.2 Model simulations

We use a zero-dimensional (box) version of the Two-Moment Aerosol Sectional (TOMAS) microphysics model (Adams and Seinfeld, 2002; Pierce and Adams, 2009; Pierce et al., 2011) combined with particle and vapor wall loss estimates to simulate the organic species phase partitioning during the FLAME III smog-chamber characterization experiments. TOMAS in this work simulates 36 logarithmically spaced size sections that span dry diameters from 3 nm to 10 μm . Simulated aerosol species include black carbon, water, and 8 lumped organic aerosol species with logarithmically spaced

5 effective saturation concentrations (C^*) between 10^{-3} to 10^4 $\mu\text{g m}^{-3}$ according to the volatility basis set (VBS, Donahue et al., 2006) based on aerosol partitioning theory (Pankow, 1994). The model simulates 8 vapor-phase species that are the vapor components of the 8 organic volatility basis set bins. Estimated molecular weights for these eight organic components followed the calculation method in Robinson et al. (2007). The model represents the CMU smog chamber as a single, well-mixed box, which implicitly assumes that mixing within the chamber occurs on faster time scales than wall losses. This fast-mixing assumption is justified as the turbulent-mixing timescale is on the order of seconds (based on $1/k_e$ derived from the Aerosol Parameterization Estimation, or APE model; see Table 1). The parameters used in our base-assumptions simulations are shown in Table 2. These parameters, as well as sensitivities of these parameters that we explore are discussed below.

15 For our base-assumption simulations as well as the sensitivity tests with perturbed parameters, we simulate all 18 smog-chamber experiments described in Table 1 using the average chamber temperature recorded during experimentation by Hennigan et al. (2011). For each simulated experiment, the initial volatility distribution of the wood-smoke POA is that proposed by May et al. (2013b) as shown in Figure 1a. May et al. (2013b) fit thermodenuder data in the 18 experiments during FLAME III mentioned above to find the optimal combination of partitioning parameters (f_i , $\Delta H_{\text{vap},i}$ and α) across the 18 experiments. ~~We test the model sensitivity to upper and lower bounds of the POA volatility distribution (representing the edges of the shaded region in Figure 6a from May et al. (2013b) and shown here in Figure 1) In the fitting procedure, May et al. (2013b) derived the volatility distribution for biomass burning in the smoke chamber using an evaporation model with the thermodenuder data as an input. They determined characterized the particle number loss in the thermodenuder by measuring the generated ammonium sulfate size distributions between using an upstream and downstream two SMPS and used then apply them the loss to correct the measured particulate organic data. However, the evaporation of semi-volatile organics due to vapor-phase wall losses may have shifted the particle volatility to lower values with time in the chamber. Thus, the volatility distribution of biomass burning adopted from May et al. (2013b) may be weighted towards lower volatilities than what those that entered the chamber, which means that vapor wall losses could be more important than what we calculated in this study. We test the model sensitivity to upper and lower bounds of their derived POA volatility distribution (representing the edges of the shaded region in Figure 6a from May et al. (2013b) and shown here in Figure 1).~~

35 Additional sources of uncertainty in modelling gas-phase wall losses are the gas-particle accommodation and gas-wall accommodation coefficients, which are used to modulate mass transfer rates between the gases and particles/walls. Different studies exploring the mass transfer rates have derived different values of the accommodation coefficients

(Greishop et al., 2007; Lee et al., 2011; Stanier et al., 2007; Saleh et al., 2013), and thus uncertainties in these accommodation coefficients need to be systematically explored in any study using models of gas-phase wall losses. In our base set of assumptions, we assume that the accommodation coefficient for mass transfer between the vapor and particle phases (α_p) is 1 based on the May et al. (2013b) results (i.e., no mass transfer limitations; Table 2). We perform sensitivity simulations wherein we assume that α_p is 0.01 and 0.001, as these values were found to be necessary to reproduce mass transfer in other studies (Grieshop et al., 2007; Stanier et al., 2007; Lee et al., 2011; Saleh et al., 2013; McVay et al., 2014). However, these lower “effective” accommodation coefficients were used in the studies of SOA formation and may not be appropriate for the POA partitioning, because we are unaware of observed mass transfer limitations in fresh POA, but they provide a logical sensitivity test. Uncertainties in the accommodation coefficients between the vapors and the wall are discussed below.

For each of the 18 experiments, we estimate the size dependent particle wall loss ($k_{w,p}(D_p)$) by applying the APE model on SMPS measurements following the procedure described in Pierce et al. (2008). Briefly, the APE model determines the best fit of the time- and size-dependent particle-phase wall loss following Eqn. 1

$$k_{w,p}(D_p) = k_{w,p0} + \frac{6\sqrt{k_e D}}{\pi R} D_1 \left(\frac{\pi \gamma_s}{2\sqrt{k_e D}} \right) + \frac{v_s}{4R/3} \quad \text{Eqn. 1}$$

where k_e (s^{-1}) is a function of the turbulent kinetic energy in the chamber (Crump and Seinfeld, 1981), D is the Brownian diffusivity of the particle of size D_p , R is the radius of the chamber, v_s is the gravitational settling velocity of the particle, and $k_{w,p0}$ is a size-independent wall-loss rate that is used to represent the effect of electrostatic forces on the wall loss, which tends to make particle wall losses less size dependent than turbulent wall losses would predict (Pierce et al., 2008). D_1 is the Debye function (Aramowitz and Stegun, 1964). We use non-linear least squares fitting optimization to best estimate the condensation/evaporation and wall-loss parameters in the APE model. The goal of fitting optimization is to minimize χ^2 as follows:

$$\chi^2 = \sum_{a=1}^3 \left(\frac{M_{i(a),p} - M_{i(a),o}}{M_{i(a),o}} \right)^2 \quad \text{Eqn.2}$$

where $i(a)$ is the set of total diameter moments (0, 1.5, 3). The chosen range of moments ensures the model fits both the total number (0th moment) and the total volume (proportional to the 3rd moment). The subscripts p and o indicate the predicted and observed moments, respectively. Derived k_{w0} and k_e for 18 experiments are listed in Table 1. Calculated wall loss rates (k_w , s^{-1}) for the 18 experiments are generally consistent with each other as shown in Figure S2. For times when the SMPS is sampling from the thermodenuder (rather than directly from the bag), we linearly interpolated the concentration in each SMPS size bin in time between the previous and

following measurement made directly from the bag. Further, to reduce noise in the APE model, we smooth the concentration in each SMPS size section (both the direct measurements and interpolated data) using a 9-point moving time average. SMPS data for times when the thermodenuder was bypassed are linearly interpolated for the APE fits (and throughout this study). Further, the SMPS data are smoothed by 9-point moving average between each bin for the APE model to reduce noise in the time-dependent wall loss rates. Table 1 lists the derived k_e and $k_{w,p0}$ for the 18 experiments.

In the simulations, we assume vapor wall loss to be reversible. The rate coefficient for gross transfer of gas-phase species onto the walls is described as $k_{w,on}$ (McMurry and Grosjean, 1985; Zhang et al., 2014):

$$k_{w,on} = \left(\frac{A}{V}\right) \frac{\left(\frac{\alpha_w \bar{c}}{4}\right)}{1.0 + \left(\frac{\pi}{2}\right) \left[\frac{\alpha_w \bar{c}}{4(k_e D_{gas})^{0.5}}\right]} \quad \text{--- Eqn.}$$

23

where A/V is the surface to volume ratio of the chamber, α_w is the mass accommodation coefficient of vapors onto the chamber walls, \bar{c} (m s^{-1}) is the mean thermal speed of the molecules (calculated using the molecular weights of each organic volatility bin), k_e is a function of the turbulent kinetic energy in the chamber (derived from the APE model described above), and D_{gas} is the molecular diffusivity ($\text{m}^2 \text{s}^{-1}$). As a base assumption for the accommodation coefficient α_w , we assume 1×10^{-5} , adopted from Matsunaga and Ziemann (2010), for all volatility bins. We perform sensitivity simulations where 1) we use alternate accommodation coefficient values that depend on volatility, based on Zhang et al. (2015) and as shown in Table 3 and 2) take constant values of 1×10^{-4} , 1×10^{-2} and 1, respectively, to explore the uncertainty in the accommodation coefficients as shown in Table 3.

The gross evaporation rate coefficient from the wall is $k_{w,off}$ (Matsunaga and Ziemann, 2010):

$$k_{w,off} = \frac{k_{w,on}}{K_w C_w} = k_{w,on} \left(\frac{C^* M_w \gamma_w}{C_w M_p \gamma_p}\right) \quad \text{--- Eqn.}$$

34

where K_w is the gas-particle partitioning coefficient, C_w is the equivalent or effective organic mass concentration of the walls (in units of mass per chamber volume), C^* is the saturation concentration ($\mu\text{g m}^{-3}$), M_p and M_w are the average molecular weights of the organic species in the particles and in the Teflon film comprising the chamber ($\mu\text{g m}^{-3}$), and γ_w and γ_p are the activity coefficients of the organic species in the Teflon film and the particle, respectively. γ_p is assumed to be unity. $C_w/M_w \gamma_w$ was measured to be 9, 20,

50 and 120 $\mu\text{mole m}^{-3}$ for n-alkanes, 1-alkenes, 2-alcohols, and 2-ketones, respectively (Matsunaga and Ziemann, 2010). C_w was also found to have positive correlation with volatility of organics, spanning 5 orders in Zhang et al. (2015). As our base assumption, we use 120 $\mu\text{mole m}^{-3}$ for this parameter. We also perform sensitivity simulations where we assume the values of 9, 20, 50 $\mu\text{mole m}^{-3}$ and $C_w/M_w\gamma_w$ as ~~the a~~ function of C_i^* (following Zhang et al. 2015) in a series of sensitivity tests. The $k_{w,off}$ values for each volatility bin using 120, 9 $\mu\text{mole m}^{-3}$ and varying $C_w/M_w\gamma_w$ are shown in Table 3. Finally, in our base simulations, we assume that the modelled particles and vapors are in equilibrium at the start of the experiment in the CMU smog chamber. However, as the CMU chamber was filled, smoke from the FSL burning chamber was diluted by ~25:1, which would make the vapor-phase organics sub-saturated with respect to the particle phase. As a sensitivity test, we assume that particles and vapor are in equilibrium in the FSL burning chamber, and that the CMU smog chamber is filled instantly as the FSL smoke is diluted by 25:1. It is not clear if this sensitivity study is a better assumption than our base assumption (particles and vapors start in equilibrium in the CMU chamber) as the CMU smog chamber was actually filled over 30 minutes and thus particles and vapors will move towards equilibrium (and particles and vapors will also be lost to the walls) during these 30 minutes. However, since we do not know the actual vapor-phase concentrations at the time when the CMU chamber is full and particle-phase measurements start, we are left with these two assumptions for bounding our results. The parameters used in the TOMAS model for our base simulations are listed in Tables 1 and 2, and the properties of the 8 organic volatility bins are shown in Table 3. The sensitivity simulations that we perform are summarized in Table 4.

In addition, previous studies have assumed ~~the~~ equilibrium between semi-volatile vapors and particles deposited to the walls in the chamber studies (e.g. Weitkamp et al., 2007; Hennigan et al., 2011), as mentioned in the Introduction section. We tested the influence of this equilibrium on the OA and vapor net loss after 1hr evolution. In the test, we assume that the equilibrium between semi-volatile vapors and wall-bound particle ~~has is the~~ similar ~~behavior with to~~ that between vapors and suspended particles in the chamber, independent of the effective wall mass/wall material. ~~The condensed/evaporated vapors on the wall bound particles are thus in proportional with on the suspended particles. The condensation/evaporation of vapors to/from particles on the wall are treated as identical to suspended particles of the same size (i.e. we assume that the particles on the wall undergo identical gas-particle partitioning and mass transfer as the suspended particles). The condensed/evaporated vapors for the wall bound and suspended particles are in proportion with their particulate concentration ratio.~~ The test results show that the percent difference between the mean of basic assumption simulations and measurements across the 18 experiments is within 1%. ~~To simplify the model system, we do not consider the semi-volatile vapors/wall deposited~~

particle partitioning throughout the simulations in the study; however, we expect this to be an important uncertainty when considering SOA formation.

The buildup of wall-deposited particles and vapor on the wall of the chamber that is retained between across experiments might have impacted our observations we used to initialize and compare with our simulation results presented above. We therefore also tested modeled this potential influence in the model by estimating retaining the residue wall-deposited particles and vapors concentration and take them into account in the next experiment by repeating the same flush / fill experiment 10 times, with simulating 12 hours of "flushing" (bag the particle and vapor concentrations in the volume of the chamber continuously set to 0) between experiments. In these 10-repeat tests, the 10th experiment had an increase of 8.8% for in OM in the suspended particle phase and 2.9% for in the vapor phase due to the slow and thus incomplete evaporation of the wall-deposited compounds during the flushing process, and the resulting buildup of particles/vapor on the walls slowing vapor deposition to the walls in the subsequent "experiment" (Figure S3). These results suggest that after a number of the experiments, the accumulated wall-deposited particles and vapor in the chamber could have certain some influence on the next set of experiments even after the chamber was flushed overnight. However, since we do not know the history of the bag outside of these FLAME III experiments, we do not attempt to account for these effects in this modeling study consider the semi-volatile vapors/wall-deposited particle partitioning throughout the simulations and the influence of wall-deposited particle and vapor residue concentration on the next experiments in the study; however, this but suggest they may be represent an important uncertainty when considering in SOA formation studies and should be explored in future studies.

3 Results and discussions

3.1 Base assumption simulations of particle and vapor wall loss

Figure 2 shows the evolution of particle number, total aerosol mass, and OA mass concentrations for the simulations and measurements of the 18 experiments (symbols represent the mean values of the 18 experiments, and the error bars show the standard deviations of the variability across the 18 experiments) for the base model assumptions (Tables 1, 2 and 3). The top panels show the results for the 9 experiments with a higher initial organic mass fraction (OF, $OF > 0.8$, shown in Table 1) and the bottom panels show the 9 experiments with a lower organic fraction ($OF < 0.8$). The choice of OF of 0.8 as a cutoff was simply to split the experiments evenly. Overall, the evolution of the mean trends and standard deviations of aerosol number, mass and OA mass concentrations are captured by the model when both the particle- and vapor-phase wall losses are simulated (blue lines). Because the total time of POA characterization differed in the 18 experiments, 1 hr is used as the cutoff time to evaluate the simulation

5 results. The percent bias between the mean of these base-assumptions simulations and
measurements after 1 hr of evolution is ~~5.0-1.4%~~, ~~4.8-3.1%~~ and ~~0.4-4.8%~~ for number,
TA and OA, respectively, for the high-OF experiments and ~~5.50.94%~~, ~~436.6%~~ and ~~5.5-~~
~~0.12%~~ for the low-OF experiments (Table 5). The percent bias between the standard
10 deviations of these base-assumption simulations and measurements is ~~3.511%~~, ~~4622%~~
and ~~4521%~~ for number, TA and OA, respectively, for the high-OF experiments and
~~7.84.9%~~, ~~5031%~~ and ~~2715%~~ for the low-OF experiments (Table 5). These biases show
that the TOMAS model generally captures the number and mass loss for the high-OF
and low-OF experiments, ~~and the lower percent bias between the standard deviations~~
~~for the high-OF experiments than the low-OF experiments suggest better agreement~~
~~between simulations and measurements for high-OF experiments.~~ The measured TA
15 concentration was calculated from OA measurements using the initial OA/TA ratio,
assuming an unchanged OA/TA over the course of the experiments. This assumption
may be the reason for a high bias in TA in the low-OF burns at the end of the
simulations (panel e) because the final OA/TA ratio will be lower than the initial due to
20 vapor losses and subsequent OA evaporation. Thus the “measured TA” for the low-OF
burns should be viewed as uncertain and likely biased low.

20 Figure 3 shows the modeled evolution of organics between the particle phase, vapor
phase and the wall for the mean and standard deviation of the 18 simulations (panel a)
along with the overall mass budget and the budgets for specific processes, integrated
over the simulation (panel b). Modeled organic vapor concentrations decrease rapidly,
due to vapor loss to the walls, while mass lost due to particle deposition to the walls
is much lower in our base simulations (Figure 3a). We estimate that the organic vapor
25 concentration decreases by ~~8786±62.0%~~ of the initial vapor concentration on average,
driven by these losses to the walls and only partially compensated for by evaporation of
particles, which decreases particulate-phase mass concentrations and replenishes
some of the lost vapor. ~~3641±64.8%~~ of the total initial particulate-phase organic mass is
lost, with ~~5665%~~ of this mass loss attributed to direct particle deposition to the walls,
and ~~4435%~~ from particle evaporation driven by the wall loss of vapors (Figure 3b). The
30 removal of vapors to the walls perturbs the initial particle-gas equilibrium sub-saturating
the vapor phase with respect to the particles and thus leads to evaporation from the
particulate phase; thus ~~particle-organic wall loss and~~ particle-organic evaporation ~~have~~
~~shown the relative roughly equal importance is estimated to play a relatively important~~
~~role in the total for the~~ loss of particle-phase organic mass during the experiments under
35 our base assumptions.

Note that as long as the vapors are supersaturated with respect to the walls (i.e., $k_{\text{off}} < k_{\text{on}}$), the uptake of vapors to the wall will continue to keep the vapors subsaturated with respect to the particles, and the particles will continue to evaporate (until they have entirely evaporated). This evaporation of the particles due to vapor uptake by the walls

is analogous to the Bergeron-Findeisen process in mixed-phase clouds where liquid droplets evaporate and ice crystals grow: the vapor pressure of water with respect to ice is lower than the vapor pressure with respect to water, and in our experiments the organic vapor pressure with respect to the walls is lower than the respect to the particles. In our base-assumption calculations, $k_{\text{off}} \ll k_{\text{on}}$ throughout the experiments, which highlights the large vapor-uptake capacity of walls as discussed in Yeh and Ziemann (2014).

We perform additional tests where we turn particle and vapor losses off individually to evaluate the influence of the two mechanisms on each other (Figures 2 and 3b). When particle loss is turned off, mass loss of particles through evaporation increases by 710% over the course of the 60 min simulation, due to the higher particle surface area retained suspended in the chamber, which allows for faster evaporation. When vapor loss was-is turned off, 10% more mass was-is lost by particle wall loss than in the base simulation. Note that for the results shown in Figure 2, neither particle nor vapor wall losses alone can explain the OA or TA mass lost in the experiments using our base assumptions. On the other hand, particle wall losses alone account for the particle number concentration losses during the experiment, as expected.

The mean (across the 18 experiments) changes in the volatility distributions of organic species for the base-assumptions simulations and for the scenarios with particle and vapor wall losses on/off are shown in Figure 4. In our simulations including vapor wall losses (Figs. 4b and 4c), the vapor-phase organic species are almost entirely removed to the walls. Furthermore, the remaining particle-phase species are shifted to those with lower volatilities due to evaporation of the higher-volatility compounds (C^* of 10^2 through 10^4). The strong loss of these semi-volatile vapors, if they are SOA precursors, suggests that SOA production as observed in these wood-smoke smog-chamber experiments may have been biased low, or may have proceeded only through certain precursors that were not strongly removed by these processes. We will explore these SOA-production biases in future work.

3.2 Sensitivity tests on the model parameters

We perform a series of sensitivity tests for several model parameters to determine if the results for the base assumptions are robust to various uncertainties. As described above, our sensitivity parameters are the initial volatility distribution, the effective wall saturation concentration coefficients ($C_w/M_w\gamma_w$), the accommodation coefficients for vapor species absorbed into the walls and into particles, and the possible effects of dilution while filling the chamber (Table 4).

3.2.1 Effect of volatility distribution bounds

The upper and lower bounds of volatility distribution that we test were derived based on the experimental uncertainty in the study of May et al. (2013b). The lower- and upper-bound volatility distributions ~~corresponding to lower and higher volatility distribution~~ are shown in Figures 1b and c. Figure 5 shows the comparison of the model to the measurements for these initial distributions. The percent bias between the mean OA of these simulations and measurements is ~~-11.15%~~, ~~0.1-4.8%~~ and ~~7.12.2%~~ for the ~~lowerhigher~~-bound, base and ~~upperlower~~-bound distributions, respectively, for high-OF experiments and ~~-7.912%~~, ~~5.5-0.12%~~ and ~~135.1%~~ for low-OF experiments (Table 5). Thus, the ~~lower-bound distribution of May et al. (2013b) better estimates the high-OF experiments while the~~ best-fit distribution ~~of May et al. (2013b)~~ provides the best results ~~for the low-OF experiments in our simulations~~ (with all other parameters set to their base values). The final TA in high-volatility simulations matches the measurements better than the other volatility assumptions for the low-OF experiments; however, as discussed earlier the final measured TA in the ~~highlower~~-OF experiments is likely biased ~~lowhigh, which and this is compensated by the bias caused by the higher-~~ volatility distribution. Figure 6 shows the decrease in particle and vapor organics throughout the simulations. The lower bound volatility distribution simulations had more particle-phase organics with lower volatilities, which caused a decrease of ~~44.29%~~ in the particle-phase organic mass loss by evaporation, relative to the ~~base-base~~-case simulations. Conversely, the upper bound volatility distribution simulations have ~~23.18%~~ more particle-phase organic mass lost relative to the base-assumption simulations (~~44.48%~~ lost rather than ~~36.41%~~), due to more evaporation. While the relative importance of particle-phase wall loss versus vapor-phase wall loss followed by particle evaporation for determining total accumulated particle-organic mass loss shifts somewhat depending on the volatility distribution, both pathways of particle-phase organic mass loss have non-trivial contributions regardless of the assumed volatility distribution (Figure 6). ~~In addition, as mentioned before, since May et al. (2013b) did not consider the vapor wall loss when deriving the volatility distribution, our calculations of biomass burning. This may be weighted towards lower volatilities than what entered the chamber, which means that we may still underestimate the importance of vapor wall losses in this calculation and the uncertainty causing by attributable to the uncertainty in the volatility distribution may be larger than 18%.~~

3.2.2 Effect of $C_w/M_w\gamma_w$

$C_w/M_w\gamma_w$, the parameters describing the saturation concentration of the vapor with respect to the wall, was measured to be 9, 20, 50 and 120 $\mu\text{mole m}^{-3}$ for different organic species in Matsunaga and Ziemann (2010). ~~Our model using Varying these four reported~~ $C_w/M_w\gamma_w$ ~~over this range~~ has no significant change on the simulation (Figure 7). The simulation using the lower bound of $C_w/M_w\gamma_w$ (9 $\mu\text{mole m}^{-3}$) causes a 26% lower total amount of vapor to be lost to the wall compared with the higher bound (Figure 8),

5 because $k_{w,off}$ values are ~1 order of magnitude faster under the $9 \mu\text{mole m}^{-3}$ assumption (Table 3). Even though the net vapor loss is slowed somewhat, the mean particle-organic mass remaining at the end of the experiments is not significantly different (< 0.9% increase) from the $120 \mu\text{mole m}^{-3}$ assumption. In the study of Zhang et al. (2015), C_w was found to be highly dependent on the volatility and solubility in Teflon polymer. Use of adapted varying $C_w/M_w\gamma_w$ values (Table 3) in our model shows ~~the a~~ high bias ~~of in the~~ final ~~predicted~~ OA (~~496.3%~~ for high-OF experiments and ~~237.6%~~ for low-OF experiments) and a decrease of ~~7765%~~ ~~of in~~ the net vapor loss relative to the base-assumption simulation. The ~~contribution of the~~ evaporative OA lost to ~~the~~ wall also decreases ~~from 4435%~~ to 21% ~~in of~~ the total OA loss. ~~These are all because the adapted $C_w/M_w\gamma_w$ values from Zhang et al. (2015) are much smaller than the measurement in Matsunaga and Ziemann (2010), which increases k_{off} (Table 3) and thus lowers the vapor uptake capability of wall. These findings resulted are because the adapted $C_w/M_w\gamma_w$ values ($1.30 \times 10^{-5} - 11.1 \mu\text{mole m}^{-3}$, Table 3) for C^* bins from 10^{-3} to 10^4 from Zhang et al. (2015) are generally smaller than what we previous used in the model in the base case ($9-120 \mu\text{mole m}^{-3}$), which increases k_{off} and thus lowers the net vapor uptake to the wall.~~ Our simulations demonstrate that C_w or $C_w/M_w\gamma_w$ is an important parameter in the model, especially for vapor wall loss estimation, and use of $C_w/M_w\gamma_w$ in the range of $9-120 \mu\text{mole m}^{-3}$ captures the OA evolution in the wood-smoke chamber (when other parameters are set to their base assumptions), although this range of $C_w/M_w\gamma_w$ was measured for relatively higher volatility organic species (e.g. n-alkane, C_5-C_{16} with C^* bins of $10^5-10^9 \mu\text{g m}^{-3}$, exceeding our simulated volatility range) and ~~it~~ may not be appropriate to ~~just use a~~ single value ~~throughout the for all~~ C^* bins. To improve the model simulation and reduce the uncertainty ~~of in~~ vapor loss estimation, more ~~efforts are still work is~~ needed to ~~explore the develop~~ accurate C_w or $C_w/M_w\gamma_w$ values for organic species ~~produced in the present in~~ wood-smoke- ~~and relevant to the chamber materials used in SOA experiments chamber in the future study.~~

3.2.3 Effect of accommodation coefficients for vapor with the wall and particles

30 In our base-assumptions simulations, particle mass is lost in similar amounts via particle deposition and via evaporation (driven by vapor wall losses). This result suggests that assumptions regarding the accommodation coefficients for condensation onto the wall and/or onto particles (α_w , α_p), may influence the particle-organic mass loss via evaporation. Figures 9, 10 and 11 show how modifying the accommodation coefficients alter our simulations. In our base simulation, we assumed values of 10^{-5} and 1 for α_w and α_p , respectively as used in Matsunaga and Ziemann (2010) and May et al. (2013b). ~~To test the effects of uncertainty in α_w , we perform sensitivity studies where (1) α_w is calculated as a function of C^* , with the range from 10^{-8} to 10^{-6} as proposed by Zhang et al. (2015) and shown in Table 3, and (2) ~~we set α_w to a constant values of 10^{-4} , 10^{-2} , and 1, respectively, but keep and α_p is set to unity.~~ Figure 11 shows that~~

5 applying the lower α_w (as a function of C_i^* , from Zhang et al. (2015) ~~in the model only~~ causes only a 3.9% decrease in vapor-organics concentrations, and the vapor evaporation from particles is almost entirely suppressed because $k_{w,org}$ for C_i^* dependent α_w is several orders of magnitude lower than ~~these~~ in the base-assumptions simulation (α_w of 10^{-5} , Table 3) and thus leads to ~~the~~ negligible vapor wall loss on the 1 hr experimental timescale, compared with more substantial particle wall losses. These results are very similar to ~~the~~ our simulations with no vapor loss, and thus they lead to a high bias in final OA (12 and 14% for high- and low-OF simulations, Table 5) relative to the measurements, ~~which~~ showing that these lower α_w values may be unrealistic. For the simulations using higher α_w (10^{-4} , 10^{-2} , and 1), we find when α_w increases above 1×10^{-4} , accommodation of vapors to the wall no longer limits the vapor wall-loss rate and exerts limited influence on OA loss, as shown in Figure 11. The total OA loss increases from 41% to 47% of initial particle-phase organic mass if α_w increases from 10^{-5} to 10^{-4} , causing a lower bias ~~of~~ in the final OA (-14% and -9.5% for high- and low-OF simulations, Table 5). The proportion of OA wall loss via particle wall loss versus particle evaporation changes from 65%:35% to 52%:48%, due to increased vapor wall losses. In summary, α_w is an important factor in our calculations although its effect saturates for α_w larger than 10^{-4} . To test the effects of uncertainty in α_w , we perform a sensitivity study where α_w is calculated as a function of C_i^* as proposed by Zhang et al. (2015) and shown in Table 3, but keep α_p at unity. Figure 9 shows that this change in α_w in the model only causes a 3% decrease in vapor-organics concentrations, and the vapor evaporation from particles is almost entirely suppressed because $k_{w,org}$ is several orders lower than those used in the basic-assumptions simulation (Table 3) and thus leads to the negligible vapor wall loss on 1h experimental timescale compared with particle wall loss. These results are very similar to the simulations with no vapor loss, and thus they lead to a high bias in final OA (21% and 27% for high- and low-OF simulations, Table 5) relative to the measurements, which show that these lower α_w values may be unrealistic.

30 We also test non-unity values of α_p (0.01 and 0.001). While these non-unity α_p values have been suggested for both biogenic and anthropogenic SOA studies (Zhang et al., 2014 and McVay et al., 2014), it is not clear if these values ~~would be applied~~ are applicable to primary wood-smoke aerosol. α_p of 0.01 and 0.001 decreases the particle-organic mass loss by evaporation by 51% and 85% of the base-assumptions simulations, respectively, (Figure ~~4011~~) because the reduced α_p increases the time-scale for particle evaporation and less vapor is consequently transferred to the gas-phase. As a result, the final OA concentrations are biased high by ~~9.60.44%~~ and ~~488.3%~~ for α_p of 0.01 and 0.001 for the high-OF simulations and by ~~486.3%~~ and ~~2412%~~ for the low-OF simulations (Table 5), which ~~again~~ shows that α_p of 0.01 may be still applicable into the our study but these accommodation coefficients α_p of 0.001 may be less likely than our base assumption of unity. Thus, changing the accommodation coefficients may

significantly alter the particle mass loss by increasing the evaporation timescales; however, the changes in the accommodation coefficients from our base values may worsened the comparisons to measurements (Figures 89 and 10), depending on the combination of other parameters used in the model.

5 3.2.4 Effect of the dilution

In our base case simulations, we assume that the particles and vapors are in equilibrium at the time when the measurements started in the smog chamber. As discussed earlier, in the FLAME III experiments, the POA was diluted by ~25:1 as it was moved from the burn chamber to the smog chamber. Thus, it is possible that the vapor and particles were not in equilibrium at the start of the measurements. To test the sensitivity of our findings to the assumption that the particles and vapor were in equilibrium at the start of the measurements, we perform alternate simulations where we assume that the particles and vapor are in equilibrium prior to dilution, and the smog chamber is filled instantly with the simulation starting at this point, and thus the particles and vapor are out of equilibrium at the start of the simulation. Note that the initial total particle concentrations are still the same; however, the vapor concentrations and particle composition have changed compared to the start of the base case. As discussed earlier, it is not clear if these instant-dilution simulations are a better assumption than our base assumption of initial equilibrium because the CMU chambers were filled by the diluted air gradually over 30 minutes, and thus the system would have some time to equilibrate (and/or for particles and vapors to be lost to the walls) before the experiment started. However, we treat the instant-dilution assumption as a bounding sensitivity test to our initial-equilibrium assumption.

Figures 11 and 12 show the results of these simulations ~~where the particles were just diluted by 25:1 just prior to the start of the simulation.~~ The dilution of gas and aerosol by 25 times in the smog chamber drives the particles to evaporate. The dilution exerts no significant influence on the number loss (Figures ~~11-12~~ and ~~1213~~). The particle-organic mass lost to the walls increases by ~~6433%~~ relative to our base-assumptions simulations due to the additional evaporation from particles caused by dilution into clean air. Particle-phase wall loss decreased by ~~3320%~~ and mass loss as vapor increased by ~~486131%~~ ~~if in~~ instantaneous dilution ~~simulation is~~ compared with the base simulation (Figure ~~1213~~). Thus, whether the particles reach equilibrium after dilution into the smog chamber is an important consideration. However, the instant dilution causes OA losses to be significantly larger than the observed decreases (Figure ~~1012~~), thus this assumption is likely unrealistic for these experiments with slow dilution. On the other hand, considering that some sensitivity simulations for the accommodation coefficients (α_p and α_w) and wall saturation coefficients ($C_w/M_w\gamma_w$) showed hindered evaporation relative to the base assumptions, it is possible that the evaporation driven by dilution is dampened by lower accommodation coefficients (not shown). Thus, while our base

assumptions provided the best comparison to the measurements of the simulations tested, it is plausible that some combination of parameters may also provide simulation results that match the measurements.

3.2.5 Discussion on potential SOA-formation effects

5 The study of SOA formation in FLAME III was performed for 3-4.5 hours after POA
measurement by turning on UV light or sunlight (Hennigan et al., 2011). The light was
turned on after the particles had typically been in the chamber for ~75 minutes. SOA is
usually formed from the oxidation of the gaseous semi-volatile or intermediate-volatility
species (Nakao et al. 2011 and Yee et al., 2013). During the period prior to photo-
10 | oxidation, the concentrations of these vapors may drop by over 90% within an hour
under our base assumption (Figure 3b). Thus, vapor wall loss may have significant
influence on the SOA production. In addition, SOA is subject to the same particle- and
vapor-phase loss mechanisms as is POA during the experiments. However, due to the
15 reversible nature of vapors on the wall, vapors may be released from the wall if
significant precursor vapors are consumed by photo-oxidation. To properly estimate the
SOA production in wood-smoke plumes in the atmosphere, one must correct the
fraction of precursor vapors in the smoke that were lost to the wall and not available for
photo-oxidation, and thus the uncorrected estimates of SOA production in Hennigan et
20 al. (2011) may be an underestimate. In this work, we only simulated species with
saturation concentrations $10^4 \mu\text{g m}^{-3}$ and lower, while precursor vapors may also be at
higher saturation concentrations. Given the relationships between saturation
concentration and wall uptake that we use in the sensitivity test (Zhang et al., 2015),
higher volatility vapors may not be lost to the walls as efficiently as those in the volatility
25 range tested here. To perform the wall-loss correction for wood-smoke SOA, we must
also know which vapors (or which volatility bins) contain the precursors for SOA
formation, and thus we leave the losses of these higher volatility vapors and the
simulation of SOA formation for future work.

4. Conclusions

30 We systematically investigate particle and vapor wall losses in controlled wood-smoke
smog-chamber experiments. The semi-volatile nature of biomass-burning primary
organic aerosol means that both particles and vapors may be lost to Teflon smog
chamber walls. Vapor loss to the walls may lead to evaporation of the particles, and
may lead to a reduction in the concentration of SOA precursors in the wood-smoke
experiments.

35 We use the TOMAS microphysics box model coupled with particle and vapor wall-loss
formulations to estimate particle and vapor wall loss in 18 wood-smoke smog-chamber
chamber experiments. The TOMAS model generally captures the number and mass

loss (SMPS and AMS data) across the 18 wood-smoke chamber experiments under our base assumptions for several uncertain parameters. The percent bias between average base-assumption simulations and measurements after 1 hr of evolution is ~~5.0~~1.4%, ~~4.83~~1.1% and ~~0.4~~4.8% for number, TA (total aerosol) and OA (organic aerosol), respectively, for the high-OF (organic fraction) experiments and ~~5.50~~9.4%, ~~136.6~~% and ~~5.50~~12% for the low-OF experiments. The percent bias between the standard deviations of these base-assumption simulations and measurements is ~~3.51~~1%, ~~4622~~% and ~~4521~~% for number, TA and OA, respectively, for the high-OF experiments and ~~7.84~~9%, ~~5931~~% and ~~2715~~% for the low-OF experiments. Under the simulations with our best-guess parameters, the model estimates that the particle-organic mass loss by direct particle wall loss and organic evaporation driven by vapor wall loss are roughly equally important ~~with contributing~~ 5665% and 4435% of the total loss (average across the 18 experiments), respectively. The vapor concentration drops by ~~8786~~% of its initial value due to vapor wall loss. As a result, the volatility distribution of the remaining mass in the chamber shifts to lower volatilities by the end of the experiment.

We conducted sensitivity tests by parameter perturbation to explore uncertainties in several model inputs: the volatility distribution, the effect of assumed saturation concentrations for the wall ($C_w/M_w\gamma_w$), and the accommodation coefficients of the vapor phase organics with particles (α_p) and the wall (α_w). The model uncertainties of final OA concentration estimated using volatility distribution bounds provided in May et al. (2013) is ~~~2318~~% of the value relative to the base assumption simulations. The total organic mass loss is generally insensitive to $C_w/M_w\gamma_w$ for the range of values provided by Matsunaga and Ziemann (2010) (i.e. 9-120 $\mu\text{mole m}^{-3}$), but the vapor uptake to the walls and evaporation of particles is greatly dampened if the volatility dependent values suggested by Zhang et al. (2015) are used. α_p and α_w are demonstrated to be important parameters in the model simulation. Comparison between measurements and our simulations suggests that α_w of 10^{-5} and α_p of 1 ~~or 0.01 is the best option~~ is applicable in our wood smoke chamber simulations when other parameters were set to their base assumptions. Finally, the dilution between ~~burning chamber~~the source aerosol and the smog chamber can cause an increase of ~~6433~~% in the total particulate organic mass loss to the chamber walls, due to an increase in organic particle evaporation driven by the dilution into clean air.

While our base assumptions of the uncertain parameters provided the best comparison to measurements in the simulations tested here, it is plausible that another combination of parameters (e.g. vapors initially subsaturated with lower accommodation coefficients) may also provide agreement with the measurements. Unfortunately, without direct measurements of the semi-volatile vapors it ~~may beis not im~~possible to entirely constrain the loss processes in the chamber, so we are left to test values suggested in previous work.

As SOA from wood smoke is suspected to be formed from photo-oxidation of semi-volatile and/or intermediate-volatility species, [our studies indicate that](#) most of the SOA precursor vapors may be lost to [the](#) smog chamber walls during controlled wood-smoke SOA experiments. These vapor losses could cause [a](#) potentially ~~a~~ large underestimation of [the](#) SOA ~~produced in that may be produced in the atmosphere from~~ [oxidation of](#) wood-smoke ~~smog-chamber studies~~ [emissions](#). However, ~~to~~ further investigation [as to](#) how wall losses affect SOA production in ~~wood-smoke plumes, smog chamber studies~~ [we must also know](#) [awaits new data on precise the identities details of the](#) and volatilities [y](#) of the [key](#) precursor species, ~~and thus this is left for future work.~~

Acknowledgements. This study was supported by the Joint Fire Science Program (JFSP) under Project 14-1-03-26. We thank the Fire Lab At Missoula Experiment (FLAME) III project team and Cyle Wold, Emily Lincoln, and Wei Min Hao from the FSL for their support in organizing and conducting the FLAME-III study and for providing the dataset used here. Funding for the FLAME-III project was provided by the National Park Service, JFSP and the EPA STAR program through the National Center for Environmental Research (NCER) under grants R833747 and R834554, and DOE (BER, ASR program) DE-SC0006035.

20

References

Abramowitz, M. and Stegun, I.: Handbook of Mathematical Functions: With Formulas, Graphs, and Mathematical Tables, Courier Corporation, 1964.

Adams, P. J. and Seinfeld, J. H.: Predicting global aerosol size distributions in general circulation models, J. Geophys. Res., 107(D19), 4370, doi:10.1029/2001JD001010, 2002.

Akagi, S. K., Craven, J. S., Taylor, J. W., McMeeking, G. R., Yokelson, R. J., Burling, I. R., Urbanski, S. P., Wold, C. E., Seinfeld, J. H., Coe, H., Alvarado M. J. and Weise, D. R.: Evolution of trace gases and particles emitted by a chaparral fire in California, Atmos. Chem. Phys., 12, 1397-1421, doi :10.5194/acp-12-1397-2012, 2012.

Bond, T. C., Doherty, S. J., Fahey, D. W., Forster, P. M., Berntsen, T., DeAngelo, B. J., Flanner, M. G., Ghan, S., Kärcher, B., Koch, D., Kinne, S., Kondo, Y., Quinn, P. K., Sarofim, M. C., Schultz, M. G., Schulz, M., Venkataraman, C., Zhang, H., Zhang, S., Bellouin, N., Guttikunda, S. K., Hopke, P. K., Jacobson, M. Z., Kaiser, J. W., Klimont, Z., Lohmann, U., Schwarz, J. P., Shindell, D., Storelvmo, T., Warren, S. G. and Zender, C.

- S.: Bounding the role of black carbon in the climate system: A scientific assessment, *J. Geophys. Res. Atmos.*, 118, 5380–5552, doi:10.1002/jgrd.50171, 2013.
- Capes, G., Murphy, J. G., Reeves, C. E., McQuaid, J. B., Hamilton, J. F., Hopkins, J. R., Crosier, J., Williams, P. I., and Coe, H.: Secondary organic aerosol from biogenic VOCs over West Africa during AMMA, *Atmos. Chem. Phys.*, 9, 3841-3850, 2009.
- Chung, C. E., Ramanathan, V. and Decremer, D.: Observationally constrained estimates of carbonaceous aerosol radiative forcing, *Proc. Natl. Acad. Sci. USA*, 109, 11624-11629, doi: 10.1073/pnas.1203707109, 2012.
- Crump, J. G. and Seinfeld, J. H.: Turbulent deposition and gravitational sedimentation of an aerosol in a vessel of arbitrary shape, *J. Aerosol Sci.*, 12, 405-415, 1981.
- Cubison, M. J., Ortega, A. M., Hayes, P. L., Farmer, D. K., Day, D., Lechner, M. J., Brune, W. H., Apel, E., Diskin, G. S., Fisher, J. A., Fuelberg, H. E., Hecobian, A., Knapp, D. J., Mikoviny, T., Riemer, D., Sachse, G. W., Sessions, W., Weber, R. J., Weinheimer, A. J., Wisthaler, A., and Jimenez, J. L.: Effects of aging on organic aerosol from open biomass burning smoke in aircraft and laboratory studies, *Atmos. Chem. Phys.*, 11, 12049-12064, doi :10.5194/acp-11-12049-2011, 2011.
- DeCarlo, P. F., Slowik, J. G., Worsnop, D. R., Davidovits, P. and Jimenez, J. L.: Particle Morphology and Density Characterization by Combined Mobility and Aerodynamic Diameter Measurements. Part 1: Theory, *Aerosol Sci. Technol.*, 38, 1185-1205, 10.1080/027868290903907, 2004.
- DeCarlo, P. F., Ulbrich, I. M., Crouse, J., de Foy, B., Dunlea, E. J., Aiken, A. C., Knapp, D., Weinheimer, A. J., Campos, T., Wennberg, P. O., and Jimenez, J. L. : Investigation of the sources and processing of organic aerosol over the Central Mexican Plateau from aircraft measurements during MILAGRO, *Atmos. Chem. Phys.*, 10, 5257-5280, doi :10.5194/acp-10-5257-2010, 2010.
- Donahue, N. M., Robinson, A. L., Stanier, C. O. and Pandis, S. N.: Coupled Partitioning, Dilution, and Chemical Aging of Semivolatile Organics, *Environ. Sci. Technol.*, 40, 2635-2643, doi: 10.1021/es052297c, 2006.
- Giordano, M., Espinoza, C. and Asa-Awuku, A.: Experimentally measured morphology of biomass burning aerosol and its impacts on CCN ability, *Atmos. Chem. Phys.*, 14, 12555-12589, doi:10.5194/acp-15-1807-2015, 2015.
- Grieshop, A. P., Donahue, N. M. and Robinson, A. L.: Is the gas-particle partitioning in alpha-pinene secondary organic aerosol reversible? *Geophys. Res. Lett.*, 34, L14810, doi: 10.1029/2007GL029987, 2007.

- Grieshop, A. P., Miracolo, M. A., Donahue, N. M. and Robinson, A. L.: Constraining the Volatility Distribution and Gas-Particle Partitioning of Combustion Aerosols Using Isothermal Dilution and Thermodenuder Measurements, *Environ. Sci. Technol.*, 43, 4750-4756, doi: 10.1021/es8032378, 2009.
- 5 Hennigan, C. J., Westervelt, D. M., Riipinen, I., Engelhart, G. J., Lee, T., Collett, J. L., Pandis, S. N., Adams, P. J. and Robinson, A. L.: New particle formation and growth in biomass burning plumes: An important source of cloud condensation nuclei, *Geophys. Res. Lett.*, L09805, doi:10.1029/2012GL050930, 2012.
- 10 Hennigan, C. J., Miracolo, M. A., Engelhart, G. J., May, A. A., Presto, A. A., Lee, T., Sullivan, A. P., McMeeking, G. R., Coe, H., Wold, C. E., Hao, W.-M., Gilman, J. B., Kuster, W. C., de Gouw, J., Schichtel, B. A., Collett, J. L., Kreidenweis, S. M. and Robinson, A. L.: Chemical and physical transformations of organic aerosol from the photo-oxidation of open biomass burning emissions in an environmental chamber, *Atmos. Chem. Phys.*, 11, 7669-7686, doi :10.5194/acp-11-7669-2011, 2011.
- 15 Huffman, J. A., Docherty, K. S., Mohr, C., Cubison, M. J., Ulbrich, I. M., Ziemann, P. J., Onasch, T. B. and Jimenez, J. L.: Chemically-Resolved Volatility Measurements of Organic Aerosol from Different Sources, *Environ. Sci. Technol.*, 43, 5351-5357, doi: 10.1021/es803539d, 2009
- 20 Jacobson. M. Z. Effects of biomass burning on climate, accounting for heat and moisture fluxes, black and brown carbon, and cloud absorption effects, *J. Geophys. Res. Atmos.*, 119, 8980-9002, doi: 10.1002/2014JD021861, 2014.
- 25 Jassen, N. A. H., Gerlofs-Nijland, M. E., Lanki, T., Salonen, R. O., Cassee, F., Hoek G., Fischer, P., Brunekreef, B., Krzyzonowski, M.: Health effects of black carbon, World Health Organization, regional office for Europe, 2010. Available at: http://www.euro.who.int/data/assets/pdf_file/0004/162535/e96541.pdf. Last access at: 2015
- 30 Jathar, S. H., Gordon, T. D., Hennigan, C. J., Pye, H. O. T., Pouliot, G., Adams, P. J., Donahue, N. M. and Robinson, A. L.: Unspeciated organic emissions from combustion sources and their influence on the secondary organic aerosol budget in the United States, *Proc Natl Acad Sci USA*, 111, 10473-10478, doi: 10.1073/pnas.1323740111, 2014.
- 35 Jimenez, J. L., Canagaratna, M. R., Donahue, N. M., Prevot, A. S. H., Zhang, Q., Kroll, J. H., DeCarlo, P. F., Allan, J. D., Coe, H., Ng, N. L., Aiken, A. C., Docherty, K. S., Ulbrich, I. M., Grieshop, A. P., Robinson, A. L., Duplissy, J., Smith, J. D., Wilson, K. R., Lanz, V. A., Hueglin, C., Sun, Y. L., Tian, J., Laaksonen, A., Raatikainen, T., Rautiainen, J., Vaattovaara, P., Ehn, M., Kulmala, M., Tomlinson, J. M., Collins, D. R., Cubison, D.

- R., Dunlea, E. J., Huffman, J. A., Onasch, T. B., Alfarra, M. R., Williams, P. I., Bower, K., Kondo, Y., Schneider, J., Drewnick, F., Borrmann, S., Weimer, S., Demerjian, K., Salcedo, D., Cottrell, L., Griffin, R., Takami, A., Miyoshi, T., Hatakeyama, S., Shiono, A., Sun, J. Y., Zhang, Y. M., Dzepina, K., Kimmel, J. R., Sueper, D., Jayne, J. T.,
5 Herndon, S. C., Trimborn, A. M., Williams, L. R., Wood, E. C., Middlebrook, A. M., Kolb, C. E., Baltensperger, U. and Worsnop, D. R.: Evolution of Organic Aerosols in the Atmosphere, *Science*, 326, 1525-1529, 2009.
- Johnston, F. H., Henderson, S. B., Chen, Y., Randerson, J. T., Marlier, M., DeFries, R. S., Kinney, P., Bowman, D. M. J. S. and Brauer, M: Estimated Global Mortality
10 Attributable to Smoke from Landscape Fires, *Environ. Health. Perspect.*, 120, 695-701, 2012.
- Lee, B., Pierce, J. R., Engelhart, G. J. and Pandis, S. N.: Volatility of secondary organic aerosol from the ozonolysis of monoterpenes, *Atmos. Environ.*, 45, 2443-2452, 2011.
- Lipsky, E. M. and Robinson, A. L.: Effects of Dilution on Fine Particle Mass and
15 Partitioning of Semivolatile Organics in Diesel Exhaust and Wood Smoke, *Environ. Sci. Technol.*, 40, 155-162, doi: 10.1021/es050319p, 2006.
- Loza, C. L., Chan, A. W. H., Galloway, M., Keutsch, F. N., Flagan, R. C. and Seinfeld, J. H.: Characterization of Vapor Wall Loss in Laboratory Chambers, *Environ. Sci. Technol.*,
44, 5074-5078, doi: 10.1021/es100727v, 2010.
- 20 Matsunaga, A. and Ziemann, P. J.: Gas-Wall Partitioning of Organic Compounds in a Teflon Film Chamber and Potential Effects on Reaction Product and Aerosol Yield Measurements, *Aerosol Sci. Technol.*, 44, 881-892, 10.1080/02786826.2010.501044, 2010.
- May, A. A., Presto, A. A., Hennigan, C. J., Nguyen, N. T., Gordon, T. D. and Robinson, A. L.: Gas-particle partitioning of primary organic aerosol emissions: (1) Gasoline
25 vehicle exhaust, *Atmos. Environ.*, 77, 128-139, doi:10.1016/j.atmosenv.2013.04.060, 2013a.
- May, A. A., Levin, E. J. T., Hennigan, C. J., Riipinen, I., Lee, T., Collett, J. L., Jimenez, J. L., Kreidenweis, S. M. and Robinson, A. L.: Gas-particle partitioning of primary organic
30 aerosol emissions: 3. Biomass burning, *J. Geophys. Res. Atmos.*, 118, 11327-11338, doi:10.1002/jgrd.50828, 2013b.
- May, A. A., McMeeking, G. R., Lee, T., Taylor, J. W., Craven, J. S., Burling, I., Sullivan, A. P., Akagi, S., Collett Jr., J. L., Flynn, M., Coe, H., Urbanski, S. P., Seinfeld, J. H., Yokelson, R. J., and Kreidenweis, S. M.: Aerosol emissions from prescribed fires in the

- United States: A synthesis of laboratory and aircraft measurements, *J. Geophys. Res. Atmos.*, 119, 11826-11849, doi: 10.1002/2014JD021848, 2014.
- 5 May, A. A., Lee, T., McMeeking, G. R., Akagi, S., Sullivan, A. P., Urbanski, S., Yokelson, R. J. and Kreidenweis, S. M.: Observations and analysis of organic aerosol evolution in some prescribed fire smoke plumes, *Atmos. Chem. Phys.*, 15, 6323-6335, doi:10.5194/acp-15-6323-2015, 2015.
- McMurry, P. H. and Grosjean, D.: Gas and aerosol wall losses in Teflon film smog chambers, *Environ. Sci. Technol.*, 19, 1176-1182, doi: 10.1021/es00142a006, 1985.
- 10 McMurry, P. H. and Rader, D. J. : Aerosol Wall Losses in Electrically Charged Chambers, *Aerosol Sci. Technol.*, 4, 249-268, 10.1080/02786828508959054, 1985.
- McVay, R. C., Cappa, C. D. and Seinfeld, J. H.: Vapor–Wall Deposition in Chambers: Theoretical Considerations, *Environ. Sci. Technol.*, 48, 10251-10258, doi: 10.1021/es502170j, 2014.
- 15 Naeher, L. P., Brauer, M., Lipsett, M., Zelikoff, J. T., Simpson, C. D., Koenig, J. Q. and Smith, K. R.: Woodsmoke Health Effects: A Review, *Inhal. Toxicol.*, 19, 67-106, 2007.
- Nakao, S., Clark, C., Tang, P., Sato, K. and Cocker III, D.: Secondary organic aerosol formation from phenolic compounds in the absence of NO_x, *Atmos. Chem. Phys.*, 11, 10649-10660, doi: 10.5194/acp-11-10649-2011, 2011.
- 20 Ortega, A. M., Day, D. A., Cubison, M. J., Brune, W. H., Bon, D., de Gouw, J. A. and Jimenez, J. L.: Secondary organic aerosol formation and primary organic aerosol oxidation from biomass-burning smoke in a flow reactor during FLAME-3, *Atmos. Chem. Phys.*, 13, 11551-11571, doi: 10.5194/acp-13-11551-2013, 2013.
- Pankow, J. F.: An absorption model of gas/particle partitioning of organic compounds in the atmosphere, *Atmos. Environ.*, 28, 185-188, 1994.
- 25 Pierce, J. R., Engelhart, G. J., Hildebrandt, L., Weitkamp, E. A., Pathak, R. K., Donahue, N. M., Robinson, A. L., Adams, P. J. and Pandis, S. N.: Constraining Particle Evolution from Wall Losses, Coagulation, and Condensation-Evaporation in Smog-Chamber Experiments: Optimal Estimation Based on Size Distribution Measurements, *Aerosol Sci. Technol.*, 42, 1001-1015, doi:10.1080/02786820802389251, 2008.
- 30 Pierce, J.R., Adams, P.J., A computationally efficient aerosol nucleation/condensation method: Pseudo-steady-state sulfuric acid, *Aerosol Sci. Tech.*, 43, 216-226, 2009.
- Pierce, J. R., Riipinen, I., Kulmala, M., Ehn, M., Petäjä, T., Junninen, H., Worsnop, D. R., and Donahue, N. M., *Atmos. Chem. Phys.*, 11, 9019-9036, doi: 10.5194/acp-11-9019-2011, 2011

- 5 Platt, S.M., El Haddad, I., Zardini, A.A., Clairrotte, M., Astorga, C., Wolf, R., Slowik, J.G.,
Temime-Roussel, B., Marchand, N., Ježek, I., Drinovec, L., Močnik, G., Möhler, O.,
Richter, R., Barmet, P., Bianchi, F., Baltensperger, U. and Prévôt, A.S.H.: Secondary
organic aerosol formation from gasoline vehicle emissions in a new mobile
environmental reaction chamber, *Atmos. Chem. Phys.*, 13, 9141-9158, doi:
10.5194/acp-13-9141-2013, 2013.
- Rissler, J., Vestin, A., Swietlicki, E., Fisch, G., Zhou, J., Artaxo, P. and Andreae, M.O.:
Size distribution and hygroscopic properties of aerosol particles from dry-season
biomass burning in Amazonia, *Atmos. Chem. Phys.*, 6, 471-491, 2006.
- 10 Robinson, A. L., Donahue, N. M., Shrivastava, M. K., Weikamp, E. A., Sage, A. M.,
Greishop, A. P., Lane, T. E., Pierce, J. R. and Pandis, S. N.: Rethinking Organic
Aerosols: Semivolatile Emissions and Photochemical Aging, *Science*, 315, 1259-1262,
2007.
- 15 Sakamoto, K.M., Allan, J.D., Coe, H., Taylor, J.W., Duck, T.J. and Pierce, J.R.: Aged
boreal biomass-burning aerosol size distributions from BORTAS 2011, *Atmos. Chem.
Phys.*, 15, 1633-1646, doi: 10.5194/acp-15-1633-2015, 2015.
- 20 Saleh, R., Hennigan, C.J., McMeeking, G.R., Chuang, W.K., Robinson, E.S., Coe, H.,
Donahue, N.M. and Robinson, A.L.: Absorptivity of brown carbon in fresh and photo-
chemically aged biomass-burning emissions, *Atmos. Chem. Phys.*, 13, 7683-7693,
doi:10.5194/acp-13-7683-2013, 2013.
- Stanier, C. O., Pathak, R.K. and Pandis, S.N.: Measurements of the Volatility of
Aerosols from α -Pinene Ozonolysis, *Environ. Sci. Technol.*, 41, 2756-2763, doi:
10.1021/es0519280, 2007.
- 25 Vakkari, V., Kerminen, V., Beukes, J. P., Tiitta, P., van Zyl, P. G., Josipovic, M., Venter,
A. D., Jaars, K., Worsnop, D. R., Kulmala, M. and Laakso, L.: Rapid changes in
biomass burning aerosols by atmospheric oxidation, *Geophys. Res. Lett.*, 41, 2644–
2651, doi: 10.1002/2014GL059396, 2014.
- 30 Weitkamp, E.A., Sage, A.M., Pierce, J.R., Donahue, N.M. and Robinson, A.L.: Organic
Aerosol Formation from Photochemical Oxidation of Diesel Exhaust in a Smog
Chamber, *Environ. Sci. Technol.*, 41, 6969-6975, doi: 10.1021/es070193r, 2007.
- 35 Yee, L.D., Kautzman, K.E., Loza, C.L., Schilling, K.A., Coggon, M.M., Chhabra, P.S.,
Chan, M.N., Chan, A.W.H., Hersey, S.P., Crouse, J.D., Wennberg, P.O., Flagan, R.C.
and Seinfeld, J.H.: Secondary organic aerosol formation from biomass burning
intermediates: phenol and methoxyphenols, *Atmos. Chem. Phys.*, 13, 8019-8043, doi:
10.5194/acp-13-8019-2013, 2013.

- Yeh, G. K. and Ziemann, P. J.: Alkyl Nitrate Formation from the Reactions of C₈-C₁₄ n-Alkanes with OH Radicals in the Presence of NO_x: Measured Yields with Essential Corrections for Gas-Wall Partitioning, *J. Phys. Chem. A.*, 118, 8147-8157, 2014.
- 5 Yokelson, R.J., Crouse, J.D., DeCarlo, P.F., Karl, T., Urbanski, S., Atlas, E., Campos, T., Shinozuka, Y., Kapustin, V., Clarke, A.D., Weinheimer, A., Knapp, D.J., Montzka, D.D., Holloway, Weibring, P., Flocke, F., Zheng, W., Toohey, D., Wennberg, P.O., Wiedinmyer, C., Mauldin, L., Fried, A., Richter, D., Walega, J., Jimenez, J.L., Adachi, K., Buseck, P.R., Hall, S.R. and Shetter, R.: Emissions from biomass burning in the Yucatan, *Atmos. Chem. Phys.*, 9, 5785-5812, 2009.
- 10 Zhang, X., Cappa, C.D., Jathar, S.H., McVay, R.C., Ensberg, J.J., Kleeman, M.J. and Seinfeld, J.H.: Influence of vapor wall loss in laboratory chambers on yields of secondary organic aerosol, *Proc. Natl. Acad. Sci. USA*, 111, 5802-5807, doi: 10.1073/pnas.1404727111, 2014.
- 15 Zhang, X., Schwantes, R.H., McVay, R.C., Lignell, H., Coggon, M.M., Flagan, R.C. and Seinfeld, J.H.: Vapor wall deposition in Teflon chambers, *Atmos. Chem. Phys.*, 15, 4197-4214, doi: 10.5194/acp-15-4197-2015/4197-4214, 2015.

Table 1. Data for 18 wood smoke samples introduced to the smog chamber, including fuel types, initial number concentration measured by scanning mobility particle sizer (SMPS) and corresponding size distribution parameters (median diameter in nm and standard deviation, σ), initial total aerosol nonrefractory mass concentration as measured by the Aerodyne quadruple aerosol mass spectrometer (Q-AMS), the organic mass fraction in the aerosol phase, derived turbulence rate (k_e , s^{-1}) and size-independent particle wall-loss coefficient ($k_{w,p0}$, s^{-1}) used in the Aerosol Parameters Estimation (APE) model. The Burn ID refers to the schedule of burns in FLAME III, as reported in Hennigan et al. (2011). The initial time is taken as the end of the chamber filling period, equivalent to the start of the 75 minute mixing and characterization period, as described in the text.

Burn ID	Fuel type	Temp (K)	Initial particle number concentration (cm^{-3})	Num. size dist.		Initial total mass concentration ¹ ($\mu g m^{-3}$)	Organic mass fraction ²	$k_{w,p0}$ (s^{-1})	k_e (s^{-1})
				Median diameter (nm)	σ				
37	Lodgepole Pine	292.9	5843	157	1.73	44.96	0.943	6.688.03 ₅ $\times 10^{-5}$	1.074.84
38	Lodgepole Pine	286.8	7612	127	1.67	40.96	0.896	2.066.27 ₅ $\times 10^{-5}$	1.416.05
40	Ponderosa Pine	279.5	6505	160	1.84	63.73	0.954	3.768.67 ₅ $\times 10^{-5}$	0.693.19
42	Wire Grass	277.0	8107	123	1.55	19.63	0.484	6.921.07 ₄₅ $\times 10^{-5}$	0.772.46
43	Saw Grass	284.2	5406	123	1.73	18.16	0.347	9.841.07 ₄₅ $\times 10^{-5}$	0.527.08
45	Turkey Oak	286.3	6334	106	1.63	16.80	0.506	5.878.11 ₅ $\times 10^{-5}$	0.992.94
47	Gallberry	286.7	8265	123	1.61	39.16	0.881	7.907.37 ₅ $\times 10^{-5}$	0.190.54
49	Sage	285.0	5486	127	1.71	17.76	0.321	4.788.84 ₅ $\times 10^{-5}$	0.846.42
51	Alaskan Duff	282.5	4175	88	1.83	20.38	0.898	3.447.00 ₅ $\times 10^{-5}$	0.320.92
53	Sage	287.2	5619	132	1.76	16.09	0.348	2.318.43 ₅ $\times 10^{-5}$	0.917.57
55	White Spruce	281.6	4641	115	1.83	27.73	0.761	1.958.13 ₅ $\times 10^{-5}$	0.313.34

57	Ponderosa Pine	277.9	6624	161	1.81	72.83	0.935	5.108.43 ₅ × 10 ⁻	<u>0.964.08</u>
59	Chamise	281.9	7173	148	1.79	24.89	0.221	2.067.58 ₅ × 10 ⁻	<u>0.835.22</u>
61	Lodgepole Pine	283.1	6059	153	1.79	63.03	0.944	3.066.30 ₅ × 10 ⁻	<u>0.293.40</u>
63	Pocosin	277.9	7463	112	1.65	26.20	0.603	5.268.46 ₅ × 10 ⁻	<u>0.374.25</u>
65	Gallberry	275.3	7763	159	1.68	85.98	0.899	4.351.43 ₄ × 10 ⁻	<u>0.620.03</u>
66	Black Spruce	279.0	9828	96	1.66	35.21	0.852	3.111.02 ₄₅ × 10 ⁻	<u>0.364.42</u>
67	Wire Grass	274.5	11580	129	1.52	36.51	0.619	4.555.78 ₅₆ × 10 ⁻	<u>0.280.49</u>

¹total mass = [OA] + [SO₄²⁻] + [NO₃⁻] + [NH₄⁺] + [Cl⁻] + [BC]

²organic fraction = [OA] / ([OA] + [SO₄²⁻] + [NO₃⁻] + [NH₄⁺] + [Cl⁻] + [BC])

Table 2. Parameters used in the base-assumption simulations.

Parameter	definition	value
α_p	accommodation coefficient of vapor species on particle	1
A/V	surface-area-to-volume ratio of the chamber (m^{-1}), assuming the bag chamber to be cubic	3.14
α_w	accommodation coefficient of vapor species on the wall	1.0×10^{-5}
C_i^*	saturation concentration range ($\mu\text{g m}^{-3}$)	$[10^{-3} 10^{-2} 10^{-1} 10^0 10^1 10^2 10^3 10^4]$
$\Delta H_{vap,i}$	heat of vaporization (kJ mol^{-1})	$85 - 4 \times \log C_i^{*,1}$
M_i	species molecular weight (g mol^{-1})	$434 - 45 \times \log_{10} C_i^{*,2}$
T	Temperature (K)	Varied, according to the measurement in each burn (Table 1)

¹May, et al. (2013b)

Robinson, et al. (2007), the detailed values are shown in Table 3

Table 3. Molecular weight (g mol^{-1}) associated with each vapor pressure bin, computed for a temperature of 298K followed the calculation equation in Table 2, varying $C_w/M_w\gamma_w$ as a function of vapor pressure bins, wall loss rates (s^{-1} , $k_{w, on}$ and $k_{w, off}$ for 120, 9 $\mu\text{mol m}^{-3}$ and varying $C_w/M_w\gamma_w$) and accommodation coefficients between gas and wall (α_w) for each volatility bin in the base-assumptions simulation and the sensitivity tests.

C_i^* ($\mu\text{g m}^{-3}$)	10^{-3}	10^{-2}	10^{-1}	10^0	10^1	10^2	10^3	10^4	
Molecular weight (g mol^{-1})	569	524	479	434	389	344	299	254	
varying $C_w/M_w\gamma_w^1$	$\frac{1.30 \times 10^{-6}}{4.85 \times 10^{-6}}$	$\frac{9.16 \times 10^{-7}}{4.30 \times 10^{-6}}$	$\frac{6.44 \times 10^{-7}}{4.96 \times 10^{-5}}$	$\frac{4.53 \times 10^{-7}}{6.44 \times 10^{-4}}$	$\frac{3.18 \times 10^{-7}}{4.53 \times 10^{-3}}$	$\frac{2.24 \times 10^{-7}}{3.18 \times 10^{-2}}$	$\frac{1.572 \cdot 24 \times 10^{-4}}{1.572 \cdot 24 \times 10^{-4}}$	$\frac{11.14 \cdot 57}{11.14 \cdot 57}$	
$\alpha_{w, base}$	1.0×10^{-5}	1.0×10^{-5}							
$\alpha_{w, sens}^4$	1.80×10^{-6}	1.16×10^{-6}	7.45×10^{-7}	4.79×10^{-7}	3.08×10^{-7}	1.98×10^{-7}	1.27×10^{-7}	8.17×10^{-8}	
$k_{w, on}(\text{base}, \text{s}^{-1})$	$\frac{7.33 \times 10^{-4}}{8.11 \times 10^{-4}}$	$\frac{7.58 \times 10^{-4}}{8.41 \times 10^{-4}}$	$\frac{7.86 \times 10^{-4}}{8.76 \times 10^{-4}}$	$\frac{8.18 \times 10^{-4}}{9.16 \times 10^{-4}}$	$\frac{8.54 \times 10^{-4}}{9.62 \times 10^{-4}}$	$\frac{8.97 \times 10^{-4}}{1.02 \times 10^{-3}}$	$\frac{9.47 \times 10^{-4}}{1.08 \times 10^{-3}}$	$\frac{1.01 \times 10^{-3}}{1.16 \times 10^{-3}}$	
$k_{w, off}(\text{s}^{-1}, 120 \mu\text{mol m}^{-3})^2$	$\frac{1.07 \times 10^{-7}}{1.19 \times 10^{-4}}$	$\frac{1.21 \times 10^{-7}}{1.34 \times 10^{-9}}$	$\frac{1.37 \times 10^{-7}}{1.52 \times 10^{-9}}$	$\frac{1.57 \times 10^{-7}}{1.76 \times 10^{-8}}$	$\frac{1.83 \times 10^{-7}}{2.06 \times 10^{-7}}$	$\frac{2.17 \times 10^{-7}}{2.46 \times 10^{-6}}$	$\frac{2.64 \times 10^{-7}}{3.01 \times 10^{-5}}$	$\frac{3.31 \times 10^{-7}}{3.81 \times 10^{-4}}$	
$k_{w, off}(\text{s}^{-1}, 9 \mu\text{mol m}^{-3})^3$	$\frac{7.01 \times 10^{-7}}{1.58 \times 10^{-4}}$	$\frac{8.09 \times 10^{-7}}{1.78 \times 10^{-9}}$	$\frac{9.44 \times 10^{-7}}{2.03 \times 10^{-8}}$	$\frac{1.11 \times 10^{-6}}{2.34 \times 10^{-7}}$	$\frac{1.33 \times 10^{-6}}{2.75 \times 10^{-6}}$	$\frac{1.62 \times 10^{-6}}{3.28 \times 10^{-5}}$	$\frac{2.02 \times 10^{-6}}{4.02 \times 10^{-4}}$	$\frac{2.59 \times 10^{-6}}{5.08 \times 10^{-3}}$	
$k_{w, off}(\text{s}^{-1}, \text{varying } C_w/M_w\gamma_w)^1$	$\frac{3.95 \times 10^{-4}}{7.69 \times 10^{-4}}$	$\frac{6.31 \times 10^{-4}}{1.23 \times 10^{-3}}$	$\frac{1.02 \times 10^{-3}}{2.00 \times 10^{-3}}$	$\frac{1.67 \times 10^{-3}}{3.28 \times 10^{-3}}$	$\frac{2.76 \times 10^{-3}}{5.47 \times 10^{-3}}$	$\frac{4.66 \times 10^{-3}}{9.27 \times 10^{-3}}$	$\frac{8.04 \times 10^{-3}}{1.61 \times 10^{-2}}$	$\frac{1.43 \times 10^{-2}}{2.90 \times 10^{-3}}$	
$k_{w, on}(\text{s}^{-1}, \alpha_{w, sens})^4$	$\frac{1.55 \times 10^{-4}}{4.55 \times 10^{-4}}$	$\frac{1.05 \times 10^{-4}}{4.05 \times 10^{-4}}$	$\frac{7.15 \times 10^{-5}}{7.07 \times 10^{-5}}$	$\frac{4.86 \times 10^{-5}}{4.78 \times 10^{-5}}$	$\frac{3.31 \times 10^{-5}}{3.25 \times 10^{-5}}$	$\frac{2.27 \times 10^{-5}}{2.22 \times 10^{-5}}$	$\frac{1.56 \times 10^{-5}}{1.53 \times 10^{-5}}$	$\frac{1.09 \times 10^{-5}}{1.07 \times 10^{-5}}$	

$k_{w,off}(S^{-1}, \alpha_{w,sens})^4$	$\frac{2.27 \times 10^{-12}}{2.84 \times 10^{-16}}$	$\frac{1.68 \times 10^{-12}}{2.14 \times 10^{-15}}$	$\frac{1.24 \times 10^{-11}}{1.62 \times 10^{-14}}$	$\frac{9.32 \times 10^{-10}}{1.24 \times 10^{-13}}$	$\frac{7.09 \times 10^{-9}}{9.70 \times 10^{-13}}$	$\frac{5.50 \times 10^{-8}}{7.70 \times 10^{-12}}$	$\frac{4.36 \times 10^{-7}}{6.25 \times 10^{-14}}$	$\frac{3.59 \times 10^{-6}}{5.26 \times 10^{-10}}$
$k_{w,on}(S^{-1} \alpha_w \text{ of } 1 \times 10^2)$	2.77×10^{-3}	2.81×10^{-3}	2.85×10^{-3}	2.89×10^{-3}	2.94×10^{-3}	2.99×10^{-3}	3.05×10^{-3}	3.12×10^{-3}
$k_{w,on}(S^{-1} \alpha_w \text{ of } 1 \times 10^3)$	4.06×10^{-11}	4.47×10^{-10}	4.96×10^{-9}	5.55×10^{-8}	6.30×10^{-7}	7.25×10^{-6}	8.51×10^{-5}	1.02×10^{-3}
$k_{w,on}(S^{-1} \alpha_w \text{ of } 1 \times 10^4)$	3.99×10^{-3}	4.00×10^{-3}	4.01×10^{-3}	4.01×10^{-3}	4.02×10^{-3}	4.03×10^{-3}	4.04×10^{-3}	4.06×10^{-3}
$k_{w,on}(S^{-1} \alpha_w \text{ of } 1 \times 10^5)$	5.85×10^{-11}	6.36×10^{-10}	6.97×10^{-9}	7.70×10^{-8}	8.61×10^{-7}	9.76×10^{-6}	1.13×10^{-4}	1.33×10^{-3}
$k_{w,on}(S^{-1} \alpha_w \text{ of } 1)$	4.01×10^{-3}	4.02×10^{-3}	4.02×10^{-3}	4.03×10^{-3}	4.03×10^{-3}	4.04×10^{-3}	4.06×10^{-3}	4.07×10^{-3}
$k_{w,on}(S^{-1} \alpha_w \text{ of } 1)$	5.88×10^{-11}	6.39×10^{-10}	7.00×10^{-9}	7.73×10^{-8}	8.64×10^{-7}	9.80×10^{-6}	1.13×10^{-4}	1.34×10^{-3}

¹ $C_w/M_w \gamma_w$ as a function of saturation concentration adapted from Zhang et al. (2015)

²Upper bound and ³lower bound of $C_w/M_w \gamma_w$ derived from Matsunaga and Ziemann (2010)

⁴Accommodation coefficients adopted from Zhang et al. (2015).

Table 4. Sensitivity tests varying the input parameters.

Parameter	Range of observations
a. Volatility distribution	May et al. (2013b) best fit; upper and lower envelopes (see Figure 2 for details)
b. Effective wall saturation concentration ($C_w/M_w Y_w$, $\mu\text{mole m}^{-3}$)	9, 20, 50, and 120 for n-alkanes, 1-alkenes, 2-alcohols, and 2-ketones, respectively, after Matsunaga and Ziemann (2010) As a function of saturation concentration (C_i^*) (adapted from Zhang et al., 2015)
c. Accommodation coefficient for vapor with the wall (α_w) and particles (α_p)	Proposed as a function of saturation concentration (C_i^*) (Zhang et al., 2015) 0.01 and 0.001 as suggested by McVay et al. (2014)
d. Dilution process	Particles and vapor assumed in equilibrium before being diluted by 25:1 when filling the smog chamber. (In other simulations, the particles and vapor were assumed to be in equilibrium immediately after dilution.)

Table 5. The percent bias between the mean and the standard deviations of these simulations (including base-assumptions simulation and other sensitivity tests) and measurements after 1 hr of evolution.

	High-OF experiments			Low-OF experiments		
	Number Conc.	Total Aerosol Mass Conc.	Organic Aerosol Mass Conc.	Number Conc.	Total Aerosol Mass Conc.	Organic Aerosol Mass Conc.
Base-assumptions simulation	$\frac{1.4\% \pm 11\%}{\%} \frac{5.0 \pm 3.5}{\%}$	$\frac{3.1\% \pm 22\%}{\%} \frac{1.8 \pm 1.6}{\%}$	$\frac{4.8\% \pm 21\%}{\%} \frac{0.1 \pm 1.5}{\%}$	$\frac{0.94\% \pm 4.9\%}{\%} \frac{5.5 \pm 7.8}{\%}$	$\frac{6.6\% \pm 31\%}{\%} \frac{1.3 \pm 5.0}{\%}$	$\frac{0.12\% \pm 15\%}{\%} \frac{5.5 \pm 2.7}{\%}$
Simulation with lower bound of volatility distribution	$\frac{1.4\% \pm 11\%}{\%} \frac{4.0 \pm 7.2}{\%}$	$\frac{3.3\% \pm 13\%}{\%} \frac{8.2 \pm 1.9}{\%}$	$\frac{2.2\% \pm 11\%}{\%} \frac{1.1 \pm 1.9}{\%}$	$\frac{0.90\% \pm 4.8\%}{\%} \frac{6.1 \pm 6.3}{\%}$	$\frac{9.1\% \pm 38\%}{\%} \frac{6.6 \pm 3.9}{\%}$	$\frac{5.1\% \pm 23\%}{\%} \frac{7.9 \pm 1.4}{\%}$
Simulation with higher bound of volatility distribution	$\frac{1.6\% \pm 12\%}{\%} \frac{4.6 \pm 7.7}{\%}$	$\frac{13\% \pm 28\%}{\%} \frac{8.2 \pm 6.0}{\%}$	$\frac{15\% \pm 27\%}{\%} \frac{7.1 \pm 4.3}{\%}$	$\frac{0.94\% \pm 4.8\%}{\%} \frac{6.1 \pm 6.9}{\%}$	$\frac{0.91\% \pm 25\%}{\%} \frac{1.7 \pm 6.4}{\%}$	$\frac{-12\% \pm 6.1\%}{\%} \frac{1.3 \pm 3.9}{\%}$
Simulation using $C_w/M_w Y_w$ of 50 $\mu\text{mole m}^{-3}$	$\frac{1.4\% \pm 11\%}{\%} \frac{4.4 \pm 7.7}{\%}$	$\frac{3.0\% \pm 22\%}{\%} \frac{5.4 \pm 1.4}{\%}$	$\frac{4.6\% \pm 21\%}{\%} \frac{3.6 \pm 1.3}{\%}$	$\frac{0.93\% \pm 4.9\%}{\%} \frac{6.2 \pm 6.5}{\%}$	$\frac{6.6\% \pm 31\%}{\%} \frac{1.7 \pm 5.5}{\%}$	$\frac{0.06\% \pm 15\%}{\%} \frac{9.7 \pm 3.1}{\%}$
Simulation using $C_w/M_w Y_w$ of 20 $\mu\text{mole m}^{-3}$	$\frac{1.4\% \pm 11\%}{\%} \frac{4.4 \pm 7.4}{\%}$	$\frac{2.6\% \pm 21\%}{\%} \frac{5.8 \pm 1.3}{\%}$	$\frac{4.2\% \pm 20\%}{\%} \frac{4.1 \pm 1.2}{\%}$	$\frac{0.94\% \pm 4.8\%}{\%} \frac{6.2 \pm 6.5}{\%}$	$\frac{6.7\% \pm 32\%}{\%} \frac{1.7 \pm 5.5}{\%}$	$\frac{0.09\% \pm 15\%}{\%} \frac{9.8 \pm 3.2}{\%}$
Simulation using $C_w/M_w Y_w$ of 9 $\mu\text{mole m}^{-3}$	$\frac{1.4\% \pm 11\%}{\%} \frac{4.5 \pm 3.5}{\%}$	$\frac{2.0\% \pm 20\%}{\%} \frac{6.5 \pm 1.2}{\%}$	$\frac{3.6\% \pm 19\%}{\%} \frac{4.8 \pm 1.1}{\%}$	$\frac{0.94\% \pm 4.8\%}{\%} \frac{6.2 \pm 6.2}{\%}$	$\frac{6.8\% \pm 32\%}{\%} \frac{1.8 \pm 5.6}{\%}$	$\frac{0.34\% \pm 15\%}{\%} \frac{1.0 \pm 3.2}{\%}$
Simulation using varying $C_w/M_w Y_w$	$\frac{1.4\% \pm 11\%}{\%} \frac{4.6 \pm 8.0}{\%}$	$\frac{9.7\% \pm 9.5\%}{\%} \frac{1.9 \pm 1.2}{\%}$	$\frac{9.2\% \pm 7.4\%}{\%} \frac{1.9 \pm 1.4}{\%}$	$\frac{0.91\% \pm 4.8\%}{\%} \frac{6.1 \pm 6.7}{\%}$	$\frac{12\% \pm 38\%}{\%} \frac{2.4 \pm 6.6}{\%}$	$\frac{10.4\% \pm 24.5\%}{\%} \frac{2.3 \pm 4.5}{\%}$
Simulation using varying α_w	$\frac{1.3\% \pm 11\%}{\%} \frac{4.8 \pm 7.9}{\%}$	$\frac{12\% \pm 4.0\%}{\%} \frac{2.1 \pm 3.5}{\%}$	$\frac{12\% \pm 1.9\%}{\%} \frac{2.1 \pm 6\%}{\%}$	$\frac{0.96\% \pm 4.9\%}{\%} \frac{6.3 \pm 6.5}{\%}$	$\frac{12\% \pm 44\%}{\%} \frac{2.3 \pm 7.3}{\%}$	$\frac{14\% \pm 31\%}{\%} \frac{2.7 \pm 5.3}{\%}$
Simulation using α_w of 10^{-1}	-1.7%±12%	-11%±29%	-13%±28%	0.96%±4.9%	2.7%±25%	-8.3%±7.4%
Simulation using α_w of 10^{-2}	-1.7%±12%	-12%±30%	-14%±29%	0.91%±5.0%	2.0%±24%	-9.7%±6.2%
Simulation using α_w of	-1.7%±12%	-12%±30%	-14%±29%	0.90%±5.0%	2.0%±24%	-9.7%±6.2%

1

Simulation using
 α_p of 0.01

$\frac{1.4\% \pm 11\%}{\%} = \frac{4.6 \pm 7.8}{\%}$ $\frac{1.3\% \pm 16\%}{\%} = \frac{11 \pm 10}{\%}$ $\frac{0.44\% \pm 15\%}{\%} = \frac{9.6 \pm 8.3}{\%}$ $\frac{0.92\% \pm 4.9\%}{\%} = \frac{6.2 \pm 6.6}{\%}$ $\frac{8.0\% \pm 38\%}{\%} = \frac{19 \pm 64}{\%}$ $\frac{6.3\% \pm 22\%}{\%} = \frac{18 \pm 41}{\%}$

Simulation using
 α_p of 0.001

$\frac{1.4\% \pm 11\%}{\%} = \frac{4.6 \pm 7.6}{\%}$ $\frac{8.5\% \pm 8.1\%}{\%} = \frac{18 \pm 0.5}{\%}$ $\frac{8.3\% \pm 6.3\%}{\%} = \frac{18 \pm 1.8}{\%}$ $\frac{0.94\% \pm 4.9\%}{\%} = \frac{6.2 \pm 6.4}{\%}$ $\frac{10\% \pm 41\%}{\%} = \frac{22 \pm 69}{\%}$ $\frac{12\% \pm 28\%}{\%} = \frac{24 \pm 49}{\%}$

Simulation with
instantaneous
dilution

$\frac{2.1\% \pm 12\%}{\%} = \frac{3.2 \pm 6.5}{\%}$ $\frac{-24\% \pm 40\%}{\%} = \frac{29 \pm 42}{\%}$ $\frac{-27\% \pm 40\%}{\%} = \frac{33 \pm 42}{\%}$ $\frac{0.69\% \pm 5.2\%}{\%} = \frac{5.5 \pm 5.3}{\%}$ $\frac{-4.6\% \pm 6.7\%}{\%} = \frac{1.8 \pm 20}{\%}$ $\frac{-23\% \pm 15\%}{\%} = \frac{30 \pm 17}{\%}$

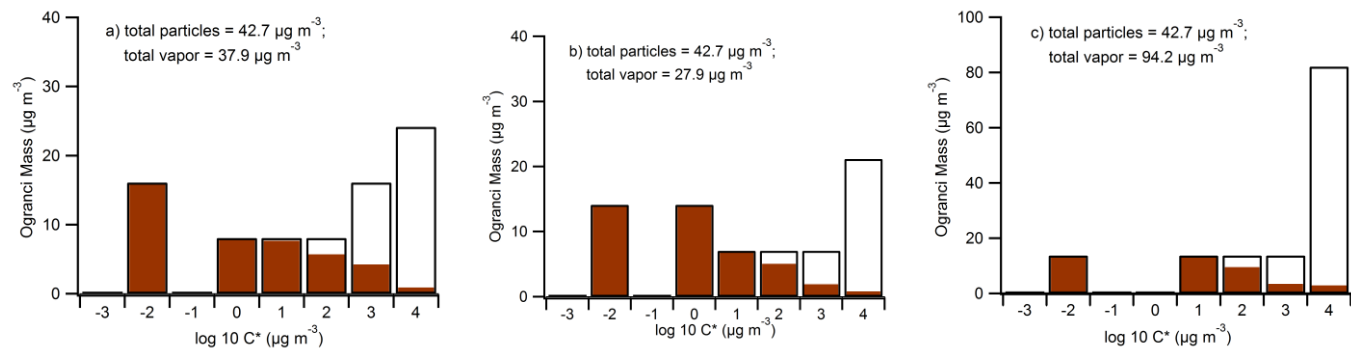


Figure 1. a) Best fit volatility distribution, b) lower bound of volatility distribution and c) upper bound of volatility distribution as reported in May et al. (2013) for a total initial average organic aerosol mass concentration of $42.7 \mu\text{g m}^{-3}$ over the 18 experiments. The shaded areas represent the organic mass in each volatility bin that is predicted to be in the aerosol phase, for average OC concentration

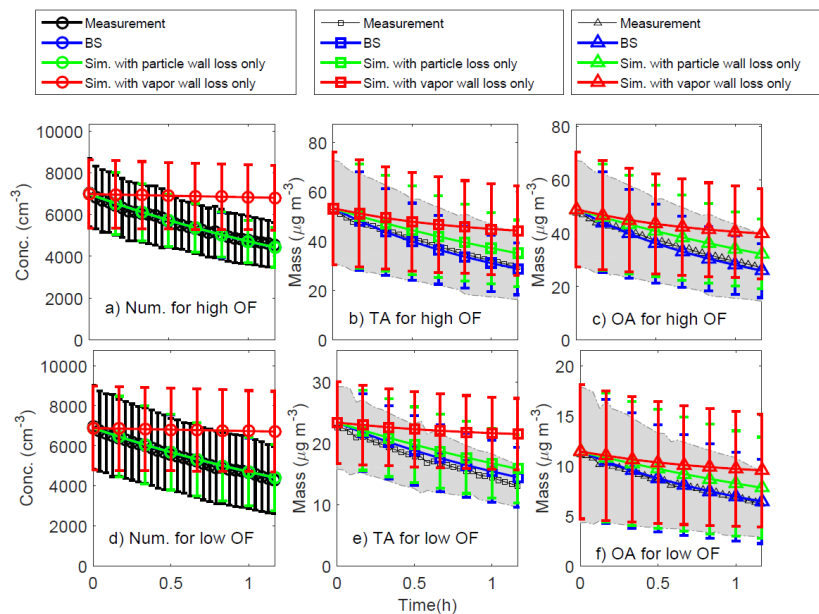


Figure 2. Comparison between the average of the measurements and the average of the model simulations of the 18 experiments for a) particle number concentration (cm^{-3}), b) total submicron aerosol mass concentration (TA, $\mu\text{g m}^{-3}$) and c) organic aerosol mass concentration (OA, $\mu\text{g m}^{-3}$) for the burns with high aerosol organic mass fraction, $\text{OF} > 0.8$; d) as in (a)-(c), but for the burns with low aerosol organic mass fraction, $\text{OF} < 0.8$. Burns with $\text{OF} > 0.8$ included burns 37, 38, 40, 47, 51, 57, 61, 65 and 66; the low OF experiments were burns 42, 43, 45, 49, 53, 55, 59, 63, and 67. The error bars and shaded areas represent one standard deviation in the measurements and the model simulations, respectively, and represent variations between the various experiments rather than uncertainties.

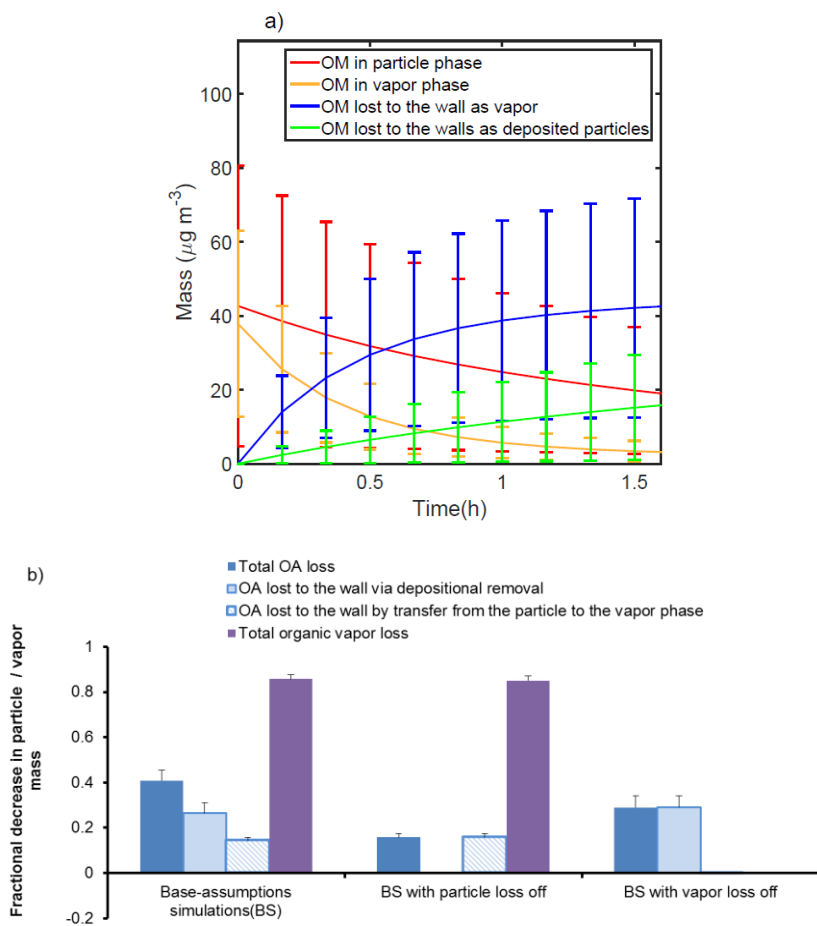


Figure 3. a) Time evolution of organic mass (OM) in the particle and vapor phases, and vapor- and particle-phase losses to the chamber walls averaged over the 18 simulations with base assumptions (in units of $\mu\text{g m}^{-3}$, the mass of particles and vapor on the wall has been normalized by the volume of the bag); b) Organic species budgets for the base simulation and two sensitivity studies. The vertical bars show the fraction of the initial assumed total organic aerosol (OA) that is removed from the chamber volume during the 75 min simulation period (blue); lost to the walls via depositional removal of particles (light blue); transferred from the particle phase to the vapor phase (blue hatched). The blue bars have been normalized by the initial particulate organic mass. The purple bars show the total fractional organic vapor that is removed from the

chamber during the simulation period. The error bars represent one standard deviation in the simulations of the 18 burns and represent burn-to-burn variability.

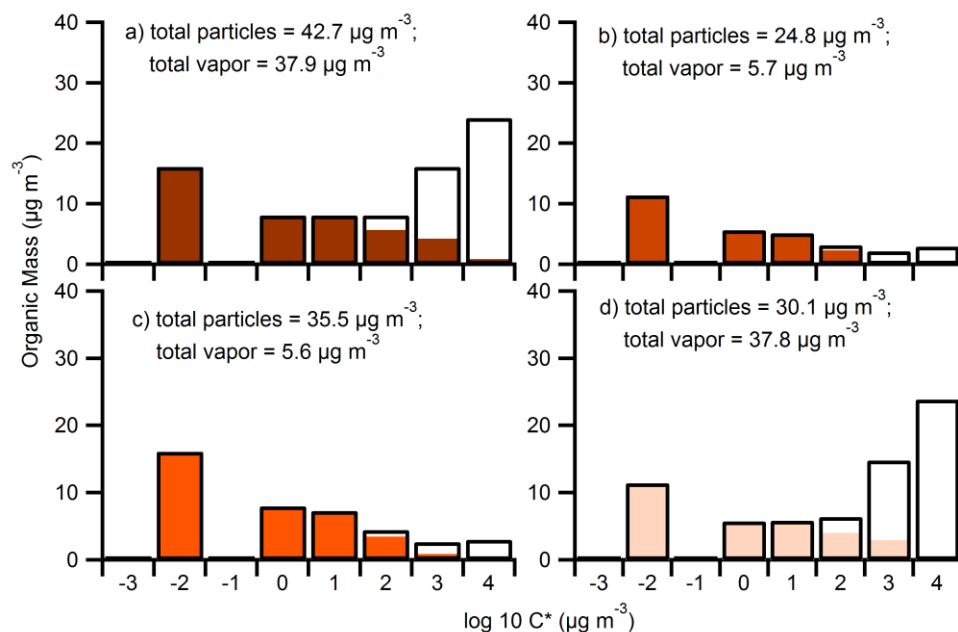


Figure 4. The total organic mass concentration, distributed into its volatility bins, at a) initial time, i.e., the distribution recommended in May et al. (2013b), for a total initial average organic aerosol mass concentration of $42.7 \mu\text{g m}^{-3}$ over the 18 experiments; and at the end of the 1h simulation for b) the base-assumptions simulations; c) the simulation in which particle losses to the walls were turned off; d) the simulation in which vapor losses to the walls were turned off. Height of bars represents the total mass expected for that volatility bin. Solid regions in the bars represent the organic mass present in the particle phase and open regions represent the mass in the vapor phase.

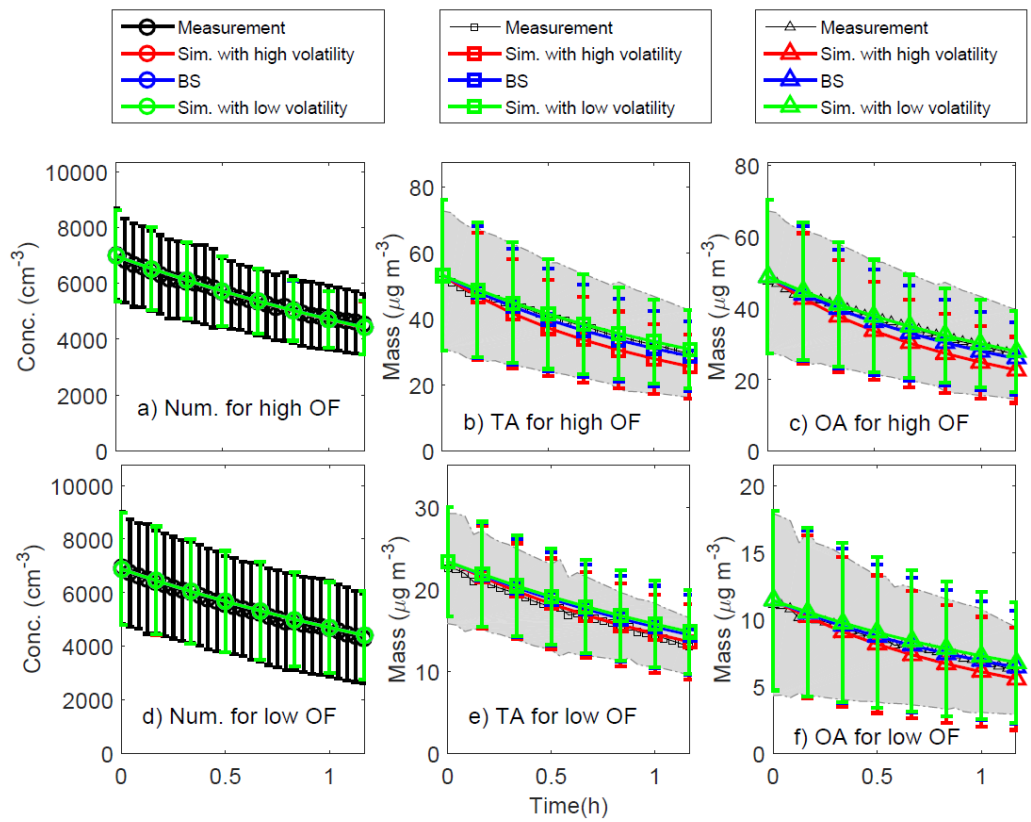


Figure 5. Similar to Figure 2 but comparing simulations with bounding initial volatilities derived from May et al. (2013b).

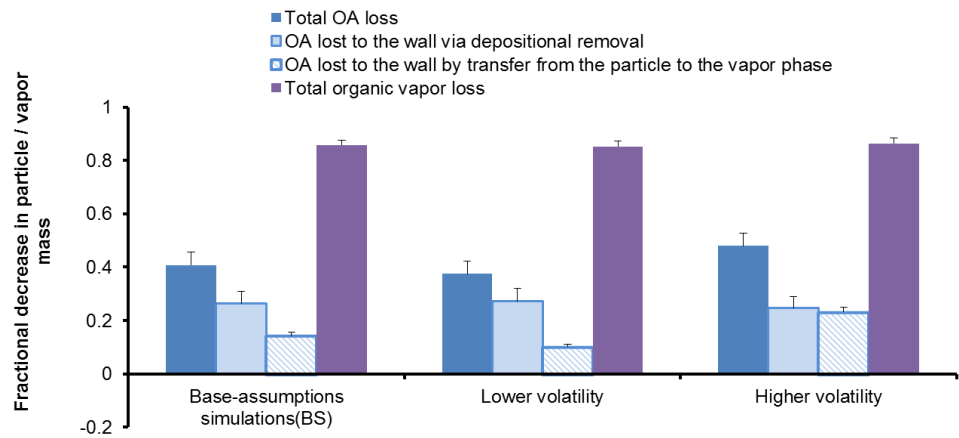


Figure 6. The organic species mass budgets for the base-assumptions simulations and two sensitivity studies using bounding volatility distributions. All other variables as in Figure 3b.

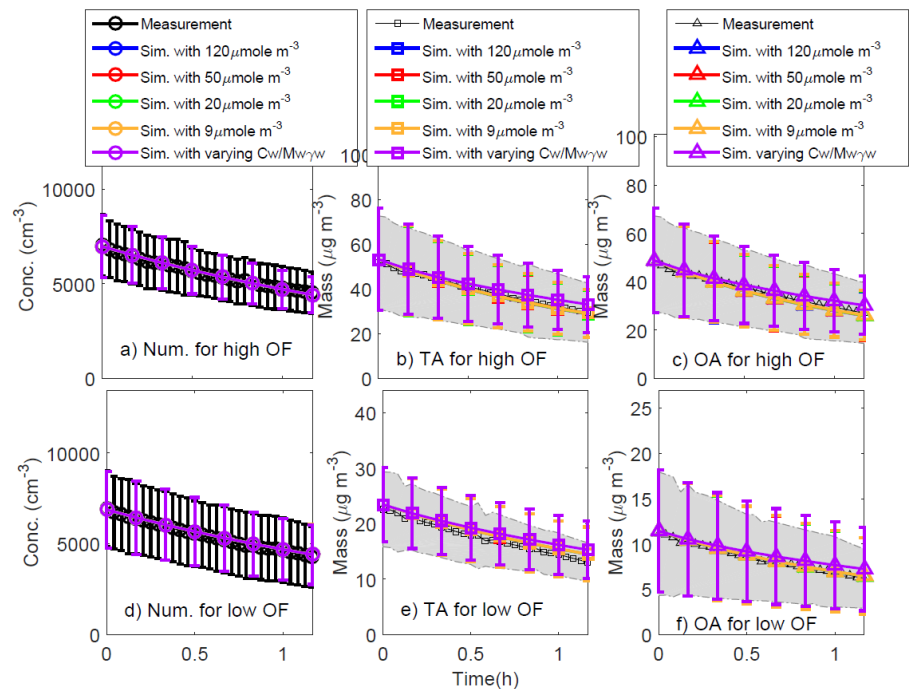


Figure 7. Similar to Figure 2 except using different $C_w/M_w\gamma_w$ of 120 (base-assumptions simulation), 50, 20, 9 $\mu\text{mole m}^{-3}$ and varying $C_w/M_w\gamma_w$ (adapted from Zhang et al. 2015).

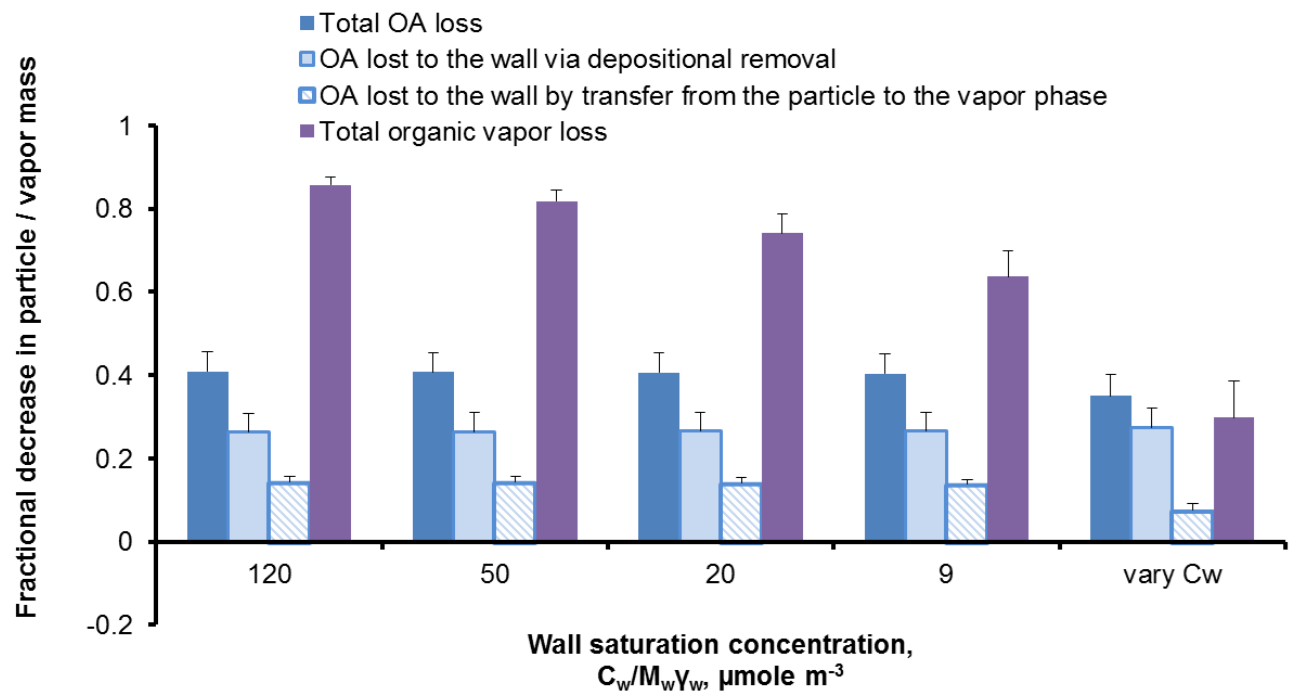


Figure 8. The organic species mass budgets for the base-assumptions simulations ($C_w/M_w\gamma_w$ of $120 \mu\text{mole m}^{-3}$) and three other sensitivity simulations using lower wall saturation concentration ($C_w/M_w\gamma_w$ of 50, 20 and $9 \mu\text{mole m}^{-3}$) and varying $C_w/M_w\gamma_w$ (adapted from Zhang et al. 2015). All other variables as in Figure 3b.

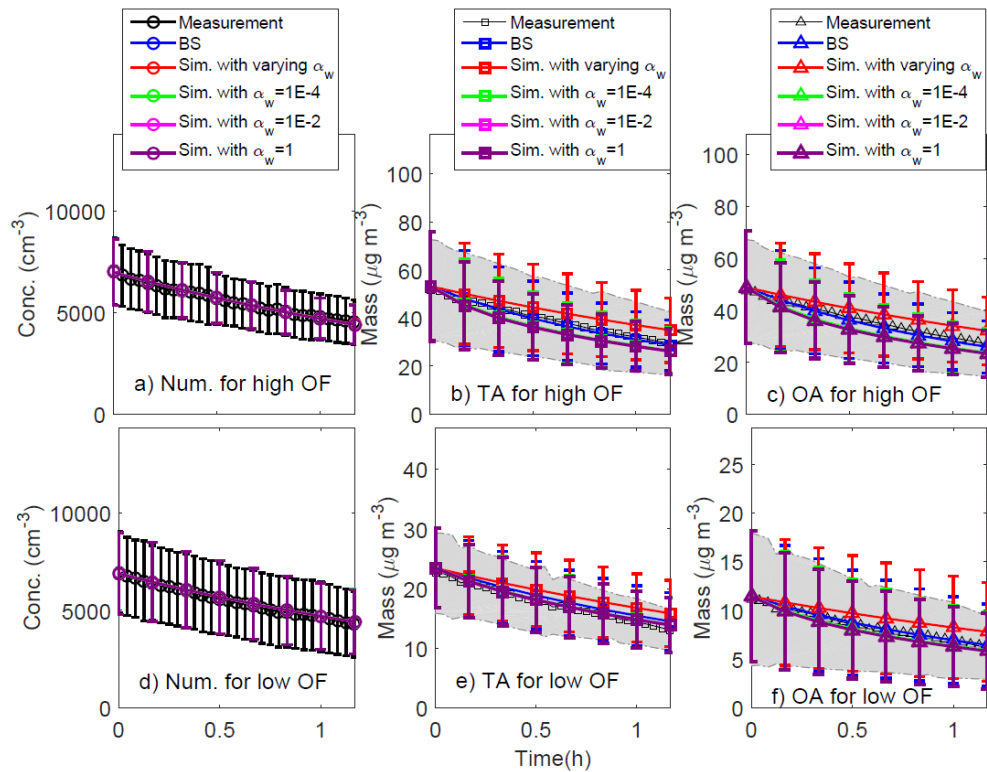


Figure 9. Similar to Figure 2 except for the simulations with different accommodation coefficients of vapor with walls, α_w , computed as a function of C_i^* (Zhang et al., 2015) and taking the values of 1×10^{-4} , 1×10^{-2} and 1. Similar to Figure 2 except for the simulations with different accommodation coefficients of vapor with walls, α_w , computed as a function of C_i^* (Zhang et al., 2014b) and accommodation coefficients of vapor with particles (α_p) of 0.01 and 0.001.

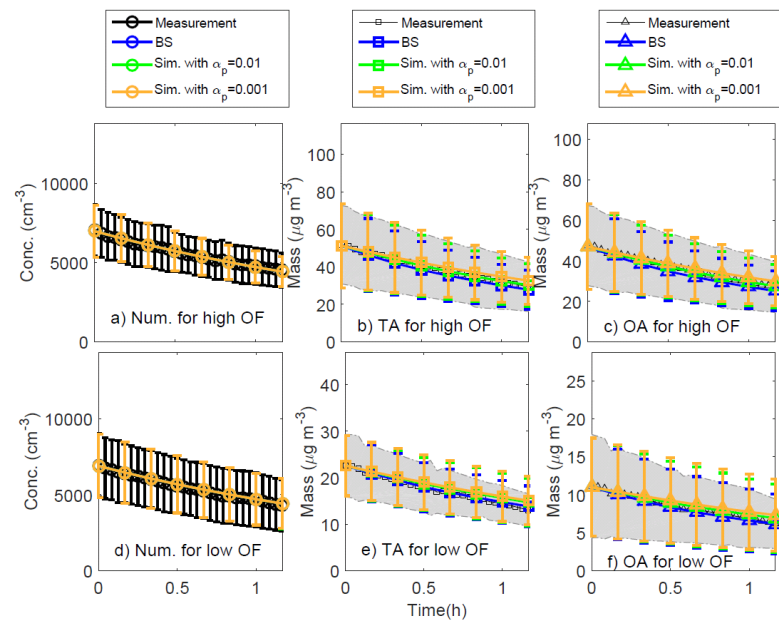


Figure 10. Similar to Figure 2 except for the simulations with different accommodation coefficients of vapor with particles (α_p) of 0.01 and 0.001.

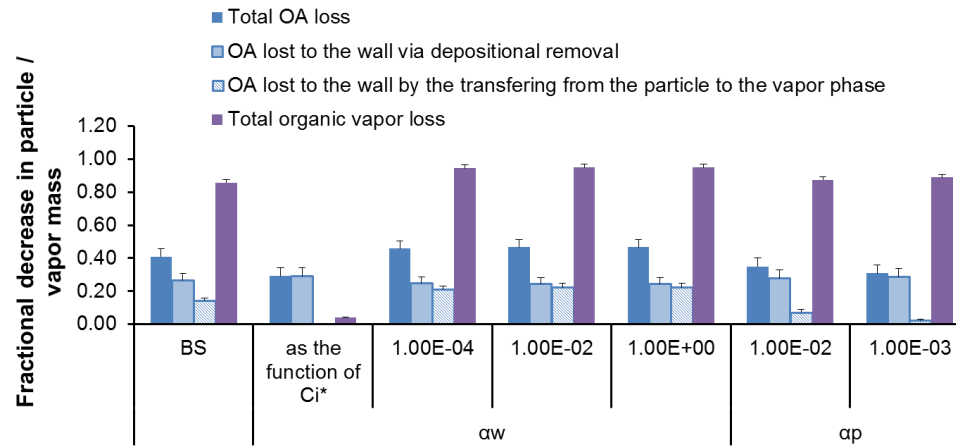


Figure 4011. The organic species mass budgets for the base-assumptions simulations (accommodation coefficient of vapor with wall (α_w) of 1×10^{-5} and accommodation coefficient of vapor with particle (α_p) of 1 and ~~three the other~~ sensitivity studies on α_w using lower wall saturation concentration (α_w) (as the function of C_i^* and of the values 1×10^{-4} , 1×10^{-2} , and 1) and α_p (of 0.01 and 0.001). All other variables as in Figure 3b.

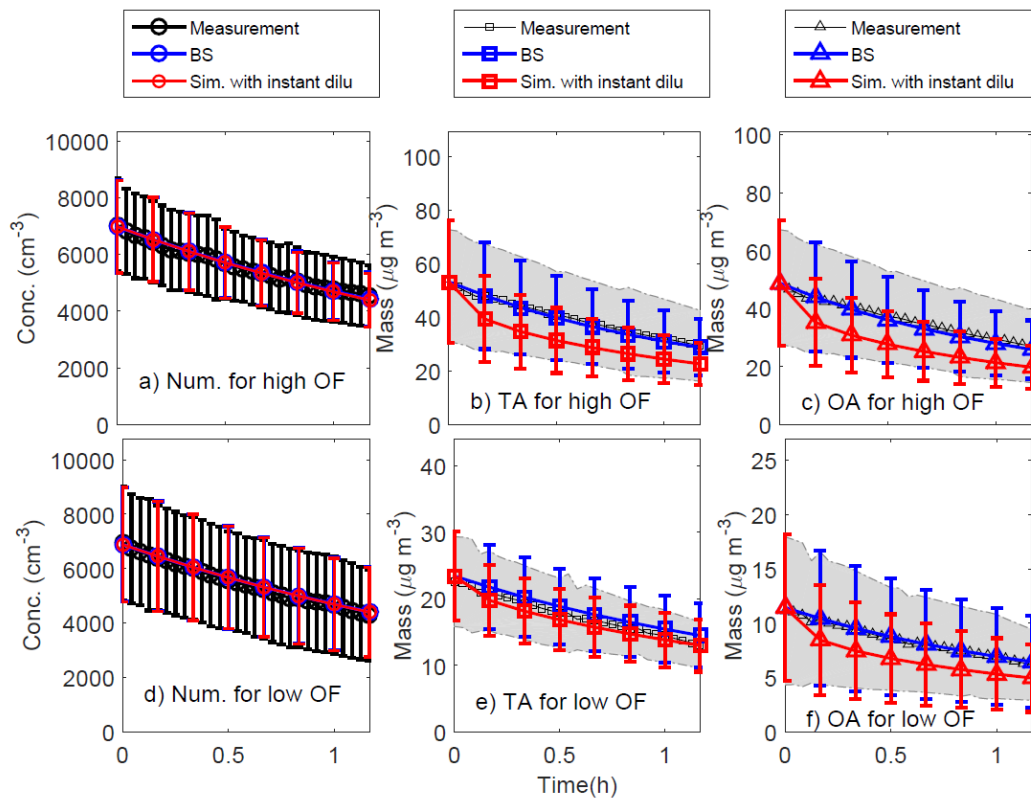
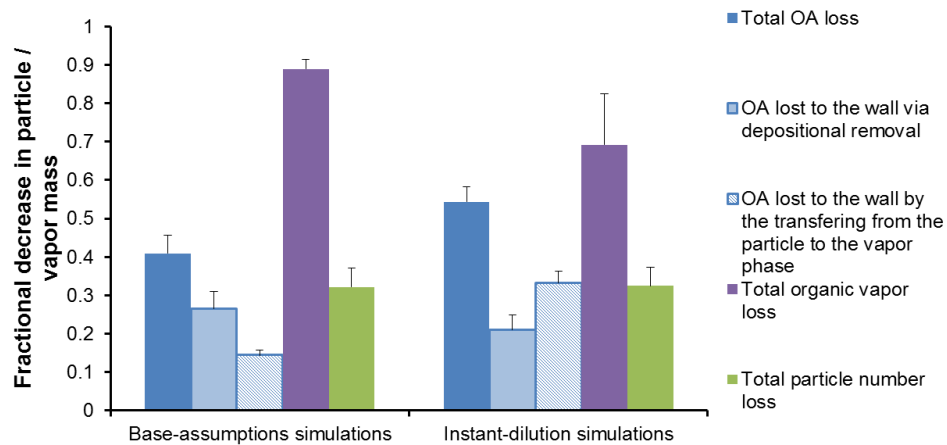


Figure 4412. Similar to Figure 2 but for the simulation with instantaneous dilution by 25:1.



Formatted: Font: (Default) Arial, 12 pt

Figure 4213. The organic species mass budgets and total number net loss for the base-assumptions simulations and instant-dilution simulations. See Figure 3b for a full description.